

The Characterization of Model Naphthenic Acid Adsorption onto
Activated Carbons: Effects of both Textural and Functional Properties

A Thesis submitted to the Committee on Graduate Studies in Partial Fulfillment of
the Requirements for the Degree of Doctor of Philosophy in the Faculty of Arts
and Science

TRENT UNIVERSITY

Peterborough, Ontario, Canada

© Copyright by Tyler M. Roy 2024

Environmental & Life Science Doctor of Philosophy Program

September 2024

Abstract

The Characterization of Model Naphthenic Acid Adsorption onto Activated Carbons: Effects of both Textural and Functional Properties

Tyler M. Roy

Naphthenic acids are a major contaminant of concern and a focus of much research around remediation of oil sand process affected waters, OSPW. Using activated carbon adsorbents are an attractive option given their low cost of fabrication and implementation. A deeper evaluation of the effect naphthenic acid structural differences have on uptake affinity is warranted. In this thesis an in-depth exploration of naphthenic acid adsorption onto activated carbon is provided including many more model naphthenic acid species than what have been assessed previously in adsorption studies. Both adsorption kinetics and isotherms at the relevant alkaline pH of OSPW using several different carbon adsorbents with pH buffering to simulate the behaviour of real OSPW were evaluated.

Given the time sensitive application of most adsorbents towards treating contaminated waters such as OSPW, achieving fast adsorption rates for model naphthenic acids is an important goal worth considering. Textural properties of activated carbon most conducive for fast adsorption kinetics were assessed using several candidate model species. Clear evidence is presented, demonstrating the influence of both the pore size distribution and particle size of

porous adsorbents on uptake rates of naphthenic acids, demonstrating that careful optimization of these adsorbent properties can result in adequate uptake rates.

Adsorption isotherms were used to assess model naphthenic acid affinity towards activated carbon. Uptake for the model naphthenic acids varied considerably regardless of the activated carbon used, ranging from 350 mg g⁻¹ to near zero highlighting recalcitrant species. The equilibrium data was explored to identify important structural features of these species and key physiochemical properties that influence adsorption. It was demonstrated that certain naphthenic acids are resistant to adsorption when hydrophobic adsorbents are used. Adsorption isotherm modelling helped explore interactions occurring at the interface between naphthenic acids and adsorbent surfaces. Naphthenic acid hydrophobicity was identified as an importance physiochemical property for achieving high adsorption capacities onto activated carbon. Evidence is also presented that indicates favorable hydrogen bonding between naphthenic acids and surface site hydroxyl groups, demonstrating the importance of adsorbent surface functionality for naphthenic acid uptake.

The adsorption mechanism was further explored through use of a thermodynamic analysis of the model naphthenic acid system using activated carbon. Standard state enthalpy and isosteric enthalpy of adsorption values were used to further support the proposed mechanisms occurring between model species and activated carbons. This research highlights the challenges associated with removing naphthenic acids from OSPW through adsorption and

identifies how adsorbent surface chemistry modification will need to be used to increase the removal efficiency of recalcitrant naphthenic acid species when using activated carbon.

Keywords

Activated Carbon, Naphthenic Acids, Isotherms, Kinetics, Modelling, Thermodynamics

Acknowledgments

First and foremost, I would like to thank my supervisor Dr. Andrew J. Vreugdenhil for his continuous support, advice, and patience throughout the completion of this thesis. I have been fortunate to have studied along side several notable individuals who have provided me with ample advice and expertise over the last several years. In particular, I would like to thank Oliver Strong and Dr. Kevin Scotland who both helped me a great deal throughout my studies. I would also like to thank everyone at the Trent Inorganic Materials Research Laboratory, including Kelly Wright, Kyle Fisher, Kyle Reyes, Sarah Begin, Elmira Nazari, and Hamant France. Additionally, I would like to thank Paul Pede from Carbonix Inc. for his support throughout this research. Thank you as well to my committee members Dr. Shegufta Shetranjiwalla-Merchant, Dr. Mark Parnis, and Dr. Steven Rafferty for their advice and input throughout my studies. Finally, I would like to express my gratitude to my family and friends for their encouragement and support throughout my studies.

Table of Contents

Abstract	ii
Acknowledgments	v
Table of Contents	vi
List of Figures	ix
List of Tables	xi
List of Equations	xii
List of Abbreviations and Symbols	xiii
1 Introduction	1
1.1 Oil Sands Process Affected Water (OSPW).....	1
1.2 Naphthenic Acids	2
1.3 Analytical Methods for Analysis of Naphthenic Acids	3
1.4 Remediation of Naphthenic Acids	4
1.4.1 Pit Lake Restoration Projects	4
1.4.2 Bioremediation	4
1.4.3 Advanced Oxidation Processes	5
1.5 Adsorption.....	5
1.5.1 Activated Carbon (AC).....	7
1.5.2 Remediation of OSPW using AC	8
1.5.3 Model Naphthenic Acid Adsorption Studies	10
1.6 Thesis Objectives	12
2 Key Experimental Techniques	13
2.1 Characterization Techniques.....	13
2.1.1 Specific Surface Area and Pore Size Distribution Analysis.....	13
2.1.2 X-Ray Photoelectron Spectroscopy (XPS) Analysis.....	15
2.1.3 Point of Zero Charge	17
2.2 Activated Carbon Synthesis	18
2.2.1 Petroleum Coke Activated Carbon	18
2.2.2 Waste Wood Activated Carbon	19
2.3 Batch Adsorption Techniques	19
2.3.1 Adsorption Kinetics.....	19

2.3.2 Adsorption Isotherms	22
2.4 Adsorption Kinetic Modelling.....	24
2.4.1 Multi-exponential Model (m-exp)	25
2.5 Adsorption Isotherm Modelling	26
2.5.1 Langmuir	26
2.5.2 Freundlich	27
2.5.3 Redlich Peterson	27
2.5.4 Sips	28
2.6 Model Evaluation	28
2.7 Adsorption Thermodynamics.....	30
2.7.1 Standard State Thermodynamic Adsorption Parameters	30
2.7.2 Isotheric Enthalpy of Adsorption.....	32
2.7.3 Activation Energy.....	33
2.8 Measurement Techniques	34
2.8.1 Total Organic Carbon (TOC) Analysis.....	34
3 Adsorption Kinetics of Model Naphthenic Acids	37
3.1 Introduction.....	37
3.2 Materials & Methods	38
3.3 Adsorption Kinetics on Physically Different Activated Carbon.....	39
3.3.1 Surface Characteristics of each Adsorbent.....	39
3.3.2 Adsorption Kinetics on each Activated Carbon.....	40
3.4 Impact of Adsorbent Physical Properties on Model Naphthenic Acid Uptake	43
3.4.1 Effect of Particle Size on Naphthenic Acid Adsorption Kinetics.....	43
3.4.2 Effect of Pore Size Distribution on Naphthenic Acid Adsorption Kinetics	46
3.5 Conclusion	49
4 Adsorption Isotherms of Model Naphthenic Acids.....	50
4.1 Introduction.....	50
4.2 Methods & Materials	52
4.2.1 Linear Modelling with Physicochemical Properties.....	52
4.3 Characterization of Activated Carbons	54
4.3.1 XPS Surface Functionality	54

4.4 Adsorption Isotherms.....	55
4.4.1 Model Evaluation of Adsorption Isotherms	58
4.5 Influence of Naphthenic Acid Physiochemical Properties on Adsorption Capacity	62
4.6 Conclusion	65
5 Adsorption Thermodynamics of Model Naphthenic Acids.....	67
5.1 Introduction.....	67
5.2 Materials & Methods	68
5.3 Activation Energy of Adsorption	69
5.4 Standard State Thermodynamic Adsorption Parameters	72
5.4.1 Langmuir Approach.....	72
5.4.2 Sips Approach.....	76
5.4.3 Isothermic Heat of Adsorption.....	78
5.5 Conclusion	80
6 Conclusions.....	82
6.1 General Conclusions	82
6.2 Future Work	83
6.3 Contributions to Science.....	84
6.3.1 Publications.....	84
6.3.2 Conferences	86
References.....	87
Appendix.....	94

List of Figures

Figure 1.1: Structure examples for classical NA species.....	2
Figure 1.2: 2D representation of porosity in activated carbon particles.	8
Figure 2.1: Survey scan showing relative elemental composition of an activated carbon surface (left). C1s and K2p high-resolution scan with synthetic component fitting of the same activated carbon surface (right).....	16
Figure 2.2: Point of zero charge calculation using the pH drift method. The intersection between the experimental pH drift (red line) and initial pH (black line) indicates charge neutrality.	17
Figure 2.3: Schematic of adsorbate transportation through a porous adsorbent to adsorption sites.	20
Figure 2.4: DPA adsorption kinetics on a phosphoric acid activated waste wood.	22
Figure 2.5: DPA adsorption isotherm on KOH activated petroleum coke.	24
Figure 2.6: Energy diagram showing the relation of E_a to ΔG°	33
Figure 3.1: Particle size distribution of each activated carbon.	40
Figure 3.2: Uptake kinetics of model NAs onto each activated carbon.....	41
Figure 3.3: Kinetic modelling using m-exp for each model NA onto PAC and HAC.....	42
Figure 3.4: Adsorption kinetics of DPA onto PACV2 with m-exp modelling. Adsorption kinetics for DPA onto CAC is shown for comparison.....	45
Figure 3.5: Adsorption kinetics of model naphthenic acids onto heat cycled petroleum coke derived activated carbon with m-exp modelling.....	47
Figure 4.1: C1s scans for (a) PAC, (b) HAC, and for (c) CAC.	55
Figure 4.2: Adsorption isotherms for each model naphthenic acid on (a) PAC, (b) HAC, (c) CAC.....	57
Figure 4.3: Maximum experimentally determined adsorption capacities of each model naphthenic acid normalized to total specific surface area of each activated carbon.	58
Figure 4.4: Relationships between the predicted distribution coefficients (logD) and predicted $\log q_e$, based on isotherm modelling for a fixed C_e of 40 mg L ⁻¹ on (a) PAC, (b) HAC, and (c) CAC.....	63
Figure 5.1: (a) Adsorption kinetics of CHA onto PAC at four different controlled temperatures. (b) kinetic modelling for CHA adsorption kinetics normalized to the predicted equilibrium capacity, a_e	69
Figure 5.2: Adsorption isotherms on PAC for a; Heptanoic acid. b; Cyclohexylacetic acid. c; Benzoic acid. Langmuir modelling is superimposed on each respective isotherm.	73
Figure 5.3: van't Hoff plot produced using the Langmuir approach for HA.....	75

Figure 5.4: Plots of $\ln C_e$ versus $1/T$ for fixed adsorption capacities, q_e , for heptanoic acid. For each fixed q_e linear regressions are displayed.....	79
Figure 5.5: Δ_{istH} versus q_e for each model naphthenic acid adsorption system.	80

List of Tables

Table 3.1: BET surface area analysis of activated carbon adsorbents used.	39
Table 3.2: Adsorption half times for model naphthenic acids onto each activated carbon based on m-exp modelling, along with fitting analysis. *CAC was not modelled by m-exp, and thus adsorption half times are direct approximations from experimental adsorption kinetics.	43
Table 3.3: BET surface area analysis of PACV2.	44
Table 3.4: Adsorption half times ($t_{1/2}$) for DPA onto different size fractions of PACV2 based on m-exp modelling along with fitting analysis. Approximate $t_{1/2}$ for DPA onto CAC is included for comparison.	46
Table 3.5: BET surface area analysis of heat cycled petroleum coke derived activated carbons.	48
Table 3.6: Adsorption half times for model naphthenic acids onto heat cycled petroleum coke derived activated carbon with fitting analysis for the m-exp model.....	Error! Bookmark not defined.
Table 4.1: Model naphthenic acids used along with predicted physicochemical properties.	53
Table 4.2: Superficial atomic % composition by XPS and point of zero (PZC). ..	54
Table 4.3: Model evaluation for adsorption isotherms of model naphthenic acids.	61
Table 4.4: Fitted parameters from isotherm modelling of the best representative models for each adsorption system.	62
Table 5.1: m-exp model fitting assessed by both the R^2 and reduced X^2 for model naphthenic acid adsorption. The time to reach 50% ($t_{1/2}$) and 75% ($t_{3/4}$) uptake, based on m-exp modelling, are shown. The m-exp model parameter showing the predicted equilibrium capacity (a_e) is also displayed.	70
Table 5.2: Calculated activation energies of adsorption (E_a) for each model naphthenic acid using two different approaches. R^2 values are included to assess linearity for the Arrhenius plot used.	71
Table 5.3: Fitting analysis and parameters obtained from Langmuir modelling of isotherms produced for each model naphthenic acid.....	74
Table 5.4: Standard state thermodynamic parameters for the adsorption of model naphthenic acids onto PAC using the Langmuir approach.	76
Table 5.5: Model parameters and fitting analysis for the Sips model fitted to each of the model naphthenic acid isotherms.	77
Table 5.6: Standard state thermodynamic parameters for model naphthenic using the Sips modelling approach.	78

List of Equations

EQ1: Material balance.....	6
EQ2: Linear BET.....	12
EQ3: Apparent surface area.....	13
EQ4: Ejected electron kinetic energy.....	14
EQ5: Multi exponential model.....	24
EQ6: Langmuir isotherm model.....	26
EQ7: Freundlich isotherm model.....	26
EQ8: Redlich Peterson isotherm model.....	27
EQ9: Sips isotherm model.....	27
EQ10: Sum of squared residuals.....	28
EQ11: Delta values for the Akaike Information Criteria.....	29
EQ12: Linear van't Hoff.....	29
EQ13: Relation between the equilibrium constant and the Langmuir constant....	30
EQ14: Relation between the equilibrium constant and the Sips constant.....	31
EQ15: Linear Clausius Clapeyron.....	31
EQ16: Rearranged Langmuir model for calculating C_e	32
EQ17: Activation energy.....	33

List of Abbreviations and Symbols

Abbreviations

OSPW	Oil Sands Process Affected Water
AEO	Acid Extractable Organics
AC	Activated Carbon
GAC	Granular Activated Carbon
UPLC-TOFMS	Ultrahigh Performance Liquid Chromatography Time-of-flight Mass Spectroscopy
TOC	Total Organic Carbon
BET	Brunauer Emmett Teller
DFT	Density Functional Theory
XPS	X-ray Photoelectron Spectroscopy
CPS	Cycles Per Second
PZC	Point of Zero Charge
PAC	Petroleum Coke Derived Activated Carbon
DPA	Diphenylacetic Acid
HAC	Wastewood Derived Activated Carbon
PFO	Pseudo First Order
PSO	Pseudo Second Order
m-exp	Multi exponential Model
R ²	Coefficient of Determination
X ²	Chi Squared
AIC _c	Corrected Akaike Information Criterion
NDIR	Non-Dispersive Near Infrared Detected
NPOC	Non Purgeable Organic Carbon
TC	Total Carbon
IC	Inorganic Carbon
DCH	Dicyclohexylacetic Acid
CHA	Cyclohexane Acetic Acid
MCH	2-methyl-1-cyclohexanecarboxylic acid
DCA	1,4-cyclohexanedicarboxylic acid
HA	Heptanoic Acid
SA	Succinic Acid
CAC	Commercial Activated Carbon
PACV2	Alternative Petroleum Coke derived Activated Carbon
PAC1	Single Activated Petroleum Coke
PAC2	Double Activated Petroleum Coke
PAC3	Triple Activated Petroleum Coke
LogD	pH Dependent Partition Coefficient
RP	Redlich Peterson
BA	Benzoic Acid

Symbols

q_t	Adsorption Capacity at time t (mg g ⁻¹)
V	Volume of solution used (L)
V_a	Volume of gas adsorbed (cm ³)
C_0	Initial concentration (mg L ⁻¹)
C_t	Concentration at time t (mg L ⁻¹)
m	Mass of adsorbent (g)
p	Set Pressure
p^0	Saturation Pressure
V_m	Monolayer Capacity (cm ³ g ⁻¹)
B_c	BET Constant
A_s	Apparent Surface Area (m ² g ⁻¹)
n_m^a	Monolayer Capacity (mmol g ⁻¹)
N_a	Avogadro's number
a_m	Area occupied by a molecule (m ² molecule ⁻¹)
E_k	Kinetic Energy of ejected electron (eV)
$h\nu$	Energy of irradiating photon (eV)
E_b	Binding Energy (eV)
ϕ	Work Function of XPS (eV)
q_e	Adsorption Capacity (mg g ⁻¹)
f_i	Fraction of kinetics curve representative of k_i
k_i	Rate constant (min ⁻¹)
a_e	Predicted adsorption capacity (mg g ⁻¹)
Q_0	Theoretical Monolayer Saturation Capacity (mg g ⁻¹)
K_L	Langmuir Constant (L mg ⁻¹)
K_F	Freundlich Constant ((mg g ⁻¹)/(L mg ⁻¹) ^{1/n})
$1/n$	Heterogeneity Factor
K_R	Redlich Peterson Constant (L g ⁻¹)
a_R	Redlich Peterson Constant (L mg ⁻¹) ^g
g	Heterogeneity Factor
Q_{mS}	Maximum Adsorption Capacity (mg g ⁻¹)
K_S	Sips Constant (L mg ⁻¹) ^{βS}
βS	Heterogeneity Factor
SSR	Sum of Squared Residuals
q_{cal}	Calculated Adsorption Capacity (mg g ⁻¹)
q_{exp}	Experimental Adsorption Capacity (mg g ⁻¹)
Δ_i	Delta Value
AIC_{c_i}	Corrected Akaike Information Criterion value for model i
$AIC_{c_{min}}$	Minimum Corrected Akaike Information Criterion value
K_c	Equilibrium Constant
ΔH°	Standard State Enthalpy (kJ mol ⁻¹)
R	Gas Constant (J K ⁻¹ mol ⁻¹)

ΔS°	Standard State Entropy ($\text{J mol}^{-1} \text{K}^{-1}$)
M_A	Molar Mass (mg mol^{-1})
C_r	Standard Reference State (mol L^{-1})
γ_e	Activity Coefficient
$\Delta_{ist}H$	Isosteric Heat of Adsorption (kJ mol^{-1})
E_a	Activation Energy (kJ mol^{-1})
A	Frequency Factor
ΔG°	Standard State Gibbs energy (kJ mol^{-1})

1 Introduction

1.1 Oil Sands Process Affected Water (OSPW)

The oil sands in Alberta Canada are composed of a bituminous suspension containing fine clays, and silica (Brown and Ulrich, 2015). Bitumen extraction requires a caustic hot water procedure resulting in significant quantities of process waters. Although recycling efforts help reduce water consumption, significant quantities of process waters are still produced annually. The concentration of contaminants such as naphthenic acids and heavy metals found naturally in the oil sands become elevated in these process waters to a point where storage in tailing ponds is required due to their high toxicity. Naphthenic acids can reach concentrations as high as 120 mg L^{-1} in oil sands process affected waters (OSPW) (Clemente and Fedorak, 2005). Although various organic contaminants such as benzene, phenol, and polycyclic aromatic hydrocarbons, are found in OSPW (Wang et al., 2013), the naphthenic acid fraction is considered the main component contributing to its toxicity (Brown and Ulrich, 2015). Li et al., provide a detailed overview of toxicity studies with naphthenic acids that have demonstrated adverse effects in a variety of organisms (Li et al., 2017). This toxicity has impeded the release or recirculation of process waters originating from the extraction process of bitumen. This has resulted in an ever-growing concern, not only over the continual accumulation of tailing ponds, but also of the approximately 895 km^2 of land disturbed from mining operations (Energy Regulator, 2019). There is also concern over

contamination of nearby environmental ecosystems, such as the Athabasca River. The growing accumulation of OSPW in Alberta, which has now well surpassed 1300 Mm³ of fluid tailings (Energy Regulator, 2019), has made naphthenic acids a high priority target for remediation efforts.

1.2 Naphthenic Acids

The targeting of naphthenic acids in OSPW has been a significant challenge due in part to the scale of the remediation efforts required, but also because of the complexity of the naphthenic acid fraction. Classically, naphthenic acids have been defined in terms of the number of carbons, n , and the degree of cyclization, z , using the formula $C_nH_{2n+z}O_2$ (Clemente and Fedorak, 2005), giving rise to mono carboxylic acids that are structurally composed of saturated cyclic and acyclic species. Examples of some naphthenic acid structures are given in **Error!**

Not a valid bookmark self-reference.. It is now well known that the classically defined naphthenic acids are only representative of a fraction of all organic acids within OSPW (Grewer et al., 2010). Varying degrees of unsaturation and aromaticity exist, and some sulfur, nitrogen, and especially oxygenated naphthenic acids have all been identified in OSPW (Headley et al., 2016). Even some tetra and penta cyclic species

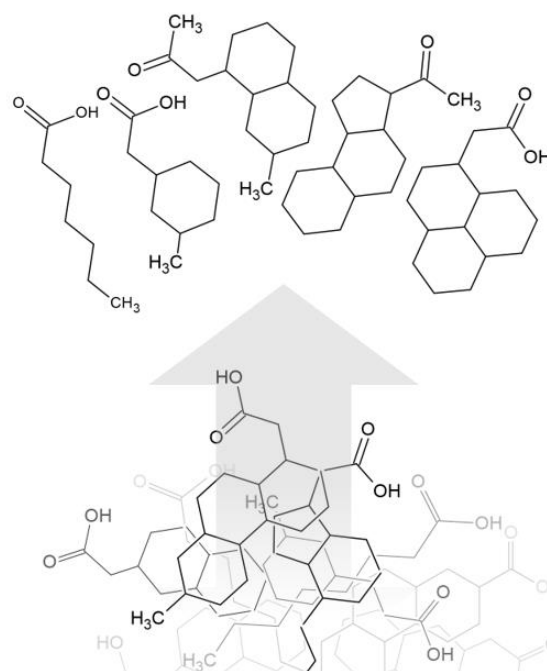


Figure 1.1: Structure examples for classical NA species.

have been identified (Rowland et al., 2011). This further emphasises the complexity of the naphthenic acid fraction, as it is now believed that thousands of individual species are expected to be present in OSPW. Thus, the treatment technologies used for naphthenic acid removal need to be capable of dealing with contaminants with a wide range of physiochemical properties.

1.3 Analytical Methods for Analysis of Naphthenic Acids

Significant progress in the development of analytical methods to characterize naphthenic acid speciation in OSPW has taken place over the last several decades. Syncrude first developed an FTIR method that involves an acidification step, followed by extraction in dichloromethane, which has now become a standard method for estimating the total concentration of acid extractable organics (AEO), which include many more organic species than those that adhere to classically defined naphthenic acids (Clemente and Fedorak, 2005). More recent attempts at using various high resolution mass spectrometry techniques have been more successful at characterizing the distribution of naphthenic acid isomer classes, by evaluating n and z numbers (Headley et al., 2013). Although some work using more comprehensive multidimensional gas chromatography instrumentation has been successful in further identifying individual naphthenic acid species (Rowland et al., 2011b, 2011a), no tool currently exists that can separate and accurately quantify each individual species, which presents a unique challenge in studying this diverse class of contaminants (Brown and Ulrich, 2015).

1.4 Remediation of Naphthenic Acids

1.4.1 Pit Lake Restoration Projects

Every oil sand mining operation in Alberta has been required since 2015 to progressively work to treat and reclaim their fluid tailings throughout their duration of operation and to have all fluid tailings fully reclaimed within 10 years of the end life cycle of these mines (Suncor Energy, 2022). Several reclamation projects are being pursued by the oil sands operators, such as end pit lake designs which will feature spent oil sands mines being transformed into aquatic ecosystems. These are long term solutions that still need considerable research to demonstrate their geochemical stability (Cossey et al., 2021). Additionally, these solutions do not currently offer a way to keep pace with the increasing deposits of OSPW that will require treatment of its organic constituents that are expected to continue to accumulate for the foreseeable future.

1.4.2 Bioremediation

Research into numerous remediation efforts have taken place for naphthenic acid removal/destruction in OSPW. Biodegradation has been an extensively studied field, largely due to the low-cost potential. Several microorganisms have been shown to be capable of biodegrading naphthenic acid species (Quinlan and Tam, 2015). Biodegradation studies have demonstrated significant removal capabilities when evaluating commercial naphthenic acid mixtures. However, a significant quantity of recalcitrant naphthenic acid species has generally been observed in OSPW upon microbial treatment. High molecular weight naphthenic acids generally are resistant to biodegradation (Brown and Ulrich, 2015). Authors

have contributed the recalcitrant nature of naphthenic acids to large extents of alkyl branching (Smith et al., 2008) and increasing degrees of cyclization (Han et al., 2008). Microbial treatment is also a slow process, with a significant fraction of naphthenic acids expected to remain in OSPW even after 10 years of treatment (Kannel and Gan, 2012).

1.4.3 Advanced Oxidation Processes

Advanced oxidation techniques, such as ozonation, have demonstrated opposing results, in which significant breakdown of high molecular weight naphthenic acids with extensive alkyl branching has been demonstrated (Xu et al., 2017). Depending upon the oxidation technique used, only limited extents of mineralization occur, with low molecular weight naphthenic acids persisting. Without complete mineralization, both biodegradation and oxidation techniques struggle to reduce OSPW toxicity to acceptable levels. More recent efforts have demonstrated the synergistic effects of combining natural OSPW microbial communities with ozonation to achieve near complete mineralization of the naphthenic acid fraction and to reduce overall toxicity to certain organisms (Wang et al., 2013). Most oxidation techniques still induce a high operational cost for OSPW treatment, which limits large scale adoption.

1.5 Adsorption

Adsorption has seen a considerable amount of attention for OSPW treatment. Instead of a destructive process, physical removal of the naphthenic acid species takes place which eliminates the possibility of more toxic by-products forming

through treatment, with the spent sorbent material acting as a permanent physical sink. A variety of adsorbents such as zeolites, bentonites, biochars, and petroleum coke, have been used to treat process waters containing naphthenic acids (Allen, 2008). Some of these, such as petroleum coke, a solid waste by-product of bitumen extraction, are representative of highly abundant, low-cost materials that are promising candidates for naphthenic acid removal (Wu et al., 2019).

Evaluation of naphthenic acid adsorption is generally assessed by batch adsorption tests, in which either processed water or a solution containing model species are mixed with a known mass of an adsorbent. The concentration of the naphthenic acids is then quantified before and after constant mixing in a closed container. Two main variations of these experiments are often included in adsorption studies. Either the time dependent uptake of naphthenic acids onto an adsorbents surface is evaluated (adsorption kinetics) or the adsorption obtained under a range of equilibrium conditions between bulk solution phase concentration and the adsorbed solid phase (adsorption Isotherm). The adsorption is often assessed via the material balance expression, which gives the mass loading of a contaminant onto the adsorbents surface.

$$q_t = \frac{V(C_0 - C_t)}{m} \quad \text{EQ1}$$

In which q_t is the time dependent adsorption capacity (mg g^{-1}) of the adsorbent. C_0 and C_t are the initial and time dependent concentrations of the naphthenic acid species in solution (mg L^{-1}), while V and m are the volume of solution and

mass of adsorbent used, respectively. In adsorption isotherms, C_t and q_t are replaced by their equilibrium equivalent C_e and q_e respectively.

1.5.1 Activated Carbon (AC)

Petcoke and most biochar adsorbents lack sufficient porosity, which limits adsorption sites and thus uptake of naphthenic acids. Activation of petcoke with chemical reagents such as KOH can yield highly porous activated carbons (AC) (Wu et al., 2018). AC can be made from nearly any carbon rich precursor. Like petcoke, many solid waste by products of industrial processes, such as various lignocellulosic materials, make for attractive low cost feedstocks for production of activated carbons (Strong et al., 2023b, 2023a; Veksha et al., 2016; Yorgun and Yildiz, 2015). Activation is usually preceded by a carbonization step, which then involves either chemical or physical inputs exposed to high temperatures. This allows for reagents such as KOH to penetrate and etch away at the defective graphene layers of these precursors, producing significant increases in the materials internal surface area (Marsh and Rodríguez-Reinoso, 2006). The extent and size of the pores that form can be carefully optimized to give specific textural properties that tailor to the removal of certain contaminants. This can give rise to both microporosity ($\leq 2 \text{ nm}$) and mesoporosity (2-50 nm), as seen in Figure 1.2. The pore size distribution and surface functionality are key variables that dictate the adsorption performance of contaminants and are thus critically optimized through careful selection of several variables, such as the starting precursors, chemical inputs and temperature programs used for activation.

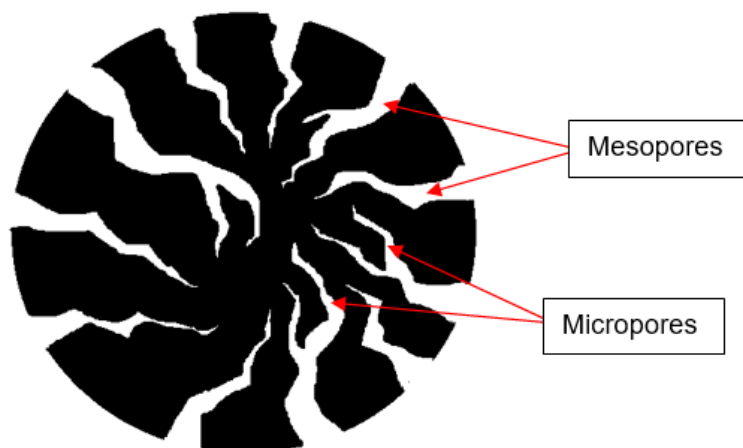


Figure 1.2: 2D representation of porosity in activated carbon particles.

1.5.2 Remediation of OSPW using AC

Several studies in recent decades have assessed the use of activated carbon to treat process waters containing naphthenic acids (Iranmanesh et al., 2014; Mònaco et al., 2022; Niasar et al., 2019). One of the more promising studies released, used steam activated delayed coke and fluid coke which both contained surface areas of approximately $500 \text{ m}^2 \text{ g}^{-1}$ (Small et al., 2012). Small and coworkers were able to demonstrate removal of >90% of the acid extractable fraction from process waters. What's more impressive was the high adsorption capacities of 515.2 mg g^{-1} and 588.8 mg g^{-1} obtained. More recently, a granular activated carbon (GAC) made from a bituminous coke activated via steam with a specific surface area nearly double that used in Small et al, has also been used to evaluate OSPW treatment, showing excellent removal (99%) of the acid extractable fraction (Islam et al., 2018). The highest adsorption capacities obtained in Islam et al, were much lower, $<100 \text{ mg g}^{-1}$, in comparison to the work done by Small and coworkers. Interestingly, Islam and coworkers used ultrahigh

performance liquid chromatography time-of-flight mass spectrometry (UPLC-TOFMS) to characterize the distribution of naphthenic acid species in terms of n and z numbers, providing some insights into the structural relationship of naphthenic acid adsorption affinity onto GAC. They found that for fixed z numbers and increasing n numbers, naphthenic acid uptake increased, while uptake decreased for decreasing z numbers and fixed n numbers. In contrast, a chemically activated petcoke adsorbent using KOH, produced by Niasar and coworkers, which had a much higher surface area of $1450 \text{ m}^2 \text{ g}^{-1}$, showed poorer removal of organics from the supernatant of OSPW (<50%) based on TOC analysis (Niasar et al., 2016). However, when acidified to a pH of 4 prior to adsorption, removal of organics was shown to reach 99%.

It's perhaps worth emphasizing that comparison between studies that use alternative methods of quantifying naphthenic acids in OSPW should be viewed with some caution. This is because methods such as TOC analysis or the commonly used FTIR analysis of the AEO fraction of OSPW produce a summed measurement of many organic species present in OSPW, which is not necessarily limited to naphthenic acids. Furthermore, even high-resolution MS techniques are semi quantitative at best, since commercial mixtures of naphthenic acids, which are known to be different from the distribution in OSPW, are used for calibration (Brown and Ulrich, 2015). Additionally, there is some evidence that filtering of OSPW via centrifugation or filtration methods prior to adsorption batch testing can influence uptake of naphthenic acids, which is worth considering when comparing studies (Azad et al., 2013). Nonetheless, all these

studies display promising results for the uptake of naphthenic acids in OSPW, but also highlight the importance of properly designed AC, as recalcitrant species are likely persisting. Although excellent removal using AC is obtained under acidic conditions, using an acidification pretreatment step with OSPW is not practical since bitumen recovery requires high alkalinity, resulting in tailings ponds at mildly alkaline pH thus complicating recycling efforts (Allen, 2008).

Tailoring an adsorbents surface to achieve a high affinity to such a diverse class of contaminants is a challenging task. Properly identifying adsorption resistant naphthenic acid species and understanding how adsorption may differ among structurally different contaminants is vital in this optimization process. Currently, the approach of working directly with OSPW while characterizing the distribution of naphthenic acids in terms of their carbon and hydrogen deficiency numbers has been useful in revealing some insights into adsorption behavior. However, there are clear limitations with this approach that hamper a more detailed evaluation of the impacts of different structural features of naphthenic acid on uptake affinity. The use of individual model naphthenic acid species with known structural differences evaluated under controlled experimental conditions provides a demonstrable way to minimize these limitations.

1.5.3 Model Naphthenic Acid Adsorption Studies

Model naphthenic acid species have been evaluated in several adsorption studies, often demonstrating excellent uptake onto activated carbon (Martinez-Iglesias et al., 2015; Niasar et al., 2018, 2016). However, only a few model species have been included in these studies, limiting how representative they

can be to a class of contaminants that generally range in molecular weight from 100 to 500 g mol⁻¹ (Wu et al., 2019). This is a critical point to make, since past adsorption studies involving OSPW have often failed to fully remove all naphthenic acid species, indicating that recalcitrant species remain. Yet model naphthenic acid adsorption studies have not properly identified what these adsorption resistant species are. Instead, work has been more focused on an evaluation of the impact of pH on adsorption affinity of model naphthenic acids. Increased adsorption affinity has generally been observed for model species when evaluated under acidic conditions, relative to the slightly alkaline pH of OSPW (Niasar et al., 2016). This improvement has been suggested to be due to the reduced solubilities of naphthenic acid species when a solution is acidified, increasing naphthenic acid affinity for the hydrophobic surface of AC. However, a more thorough characterization of model adsorption, utilizing a more structurally diverse set of surrogate compounds would greatly benefit this field as this would help better predict recalcitrant naphthenic acids species in OSPW.

In this thesis, the range of model naphthenic acid species explored has been expanded relative to what has previously been used in the literature. A significant focus has been to evaluate the adsorption mechanism for model naphthenic acids on AC and as well to identify structural features of naphthenic acids that predict recalcitrant species. This was achieved through an exploration of both adsorbent textural and functional properties, followed by a thermodynamic analysis of the model naphthenic acid adsorption process using isotherm

modelling. This approach provides key insights into the interactions occurring at the interface between activated carbon and solution.

1.6 Thesis Objectives

1. Identify the textural properties of activated carbon that are most conducive to achieving fast uptake rates of model naphthenic acids onto activated carbon.
2. Explore the structural relationship between model naphthenic acids and surface functionality of activated carbon to identify recalcitrant features of certain naphthenic acids.
3. Confirm the adsorption mechanism of model naphthenic acids through a thermodynamic analysis of adsorption onto activated carbon.

2 Key Experimental Techniques

2.1 Characterization Techniques

2.1.1 Specific Surface Area and Pore Size Distribution Analysis

The Brunauer Emmett Teller (BET) method is a surface area characterization technique that is used to provide a measurement of total surface area and the distribution of porosity for porous materials. It is fundamentally based on the usage of the BET equation to represent a gas phase adsorption isotherm. The linear form of the BET expression is shown in EQ2:

$$\frac{1}{V_a((p^0/p) - 1)} = \frac{1}{V_m B_c} + \frac{(B_c - 1)p}{V_m B_c p^0} \quad \text{EQ2}$$

This equation is an extension of the Langmuir model and was derived to interpret multilayer gas adsorption on non-porous media (Brunauer et al., 1938) and later used to describe adsorption in porous materials. Approximating surface area with this method, first requires the formation of an adsorption isotherm using an inert gas (usually nitrogen). The adsorption isotherm is produced by introducing a known amount of N₂ to a porous material which is allowed to reach adsorption equilibrium under differing relative pressures in a stepwise fashion (Condon and James B, 2006). A volumetric method is employed to measure the amount of gas adsorbed by comparing the actual pressure change in the closed system to the expected pressure change assuming the adsorbent was absent. The N₂ isotherm is produced at 77K, the boiling point of N₂, which ensures reliably measurable amounts of N₂ will be adsorbed to the materials surface (Marsh and Rodríguez-

Reinoso, 2006). Relative pressure is given as the set pressure of the closed system, p , over the saturation pressure of N₂, p^0 . Use of EQ2 is usually restricted to low relative pressure measurements (<0.3), where a linear approximation of the adsorption isotherm is suitable, thus allowing for proportionality between the left side term of EQ2, $\frac{1}{V_a((p^0/p)-1)}$ and the right side term $\frac{p}{p^0}$. This allows, V_m , the monolayer capacity of the N₂ isotherm, cm³ g⁻¹, to be determined. This is used in accordance with EQ3 to approximate the apparent surface area of the solid sample.

$$A_s = n_m^a N_a a_m \quad \text{EQ3}$$

In EQ3, n_m^a is the monolayer capacity of the material, now in units of mmol g⁻¹, while N_a is Avogadro's number, and a_m is the area occupied by the N₂ molecule, m² molecule⁻¹. Thus, knowing N_a and a_m while obtaining n_m^a from the BET isotherm modelling, the apparent surface area, often referred to as the specific surface area in m² g⁻¹, can be determined. The pore size distribution of the material is assessed through more advanced modelling techniques that utilize density functional theory (DFT) with assumed pore geometry.

2.1.1.1 BET Analysis Settings

Specific Surface area and pore size analysis was carried out on a Micromeritics Tristar II plus. The samples were analyzed using N₂ adsorption at 77 K with 104 points monitoring adsorption between $0.0065 \frac{p}{p^0}$ and $0.995 \frac{p}{p^0}$ and 52 points for desorption between $0.995 \frac{p}{p^0}$ and $0.104 \frac{p}{p^0}$. The pore size distributions were

determined using DFT with slit geometry modeling 2D-NLDFT with N₂ carbon finite pores (Jagiello and Olivier, 2009).

2.1.2 X-Ray Photoelectron Spectroscopy (XPS) Analysis

X-ray photoelectron spectroscopy or XPS, is a material characterization technique capable of evaluating the elemental composition and functionality of surfaces. X-rays irradiate a sample's surface which causes the ejection of inner shell electrons in accordance with the following expression (Skelly et al., 2014).

$$E_k = h\nu - E_b - \phi \quad \text{EQ4}$$

Where E_k is the kinetic energy of the ejected electron, $h\nu$ is the energy of the irradiating photon used by the XPS instrument, E_b is the binding energy of the ejected electron, and ϕ is the work function, which is a unique parameter for a given XPS instrument. The binding energy is directly related to the element which emits the ejected electron and, more importantly, the local chemical environment of that atom. This is observed through shifts, or small energy changes to binding energy that occur due to certain bonding geometries (Stevie and Donley, 2020). Since the energy of the X-ray and work function of the instrument are known, while the kinetic energy of the ejected electron is measured, binding energy can be determined. Thus, the chemical composition and functionality of the surface can be revealed through XPS analysis.

An example survey scan is shown in Figure 2.1 (left diagram), in which a large range of binding energies versus the relative number of ejected electrons is

measured, typically reported as counts per second (CPS). The survey scan can be used to determine the elemental composition of a materials surface, while high resolution scans of a narrow binding energy range (right diagram in Figure 2.1) can be used to determine the specific chemical composition of a given element. This requires specialized software capable of fitting the high-resolution peaks to decipher local bonding geometry and composition.

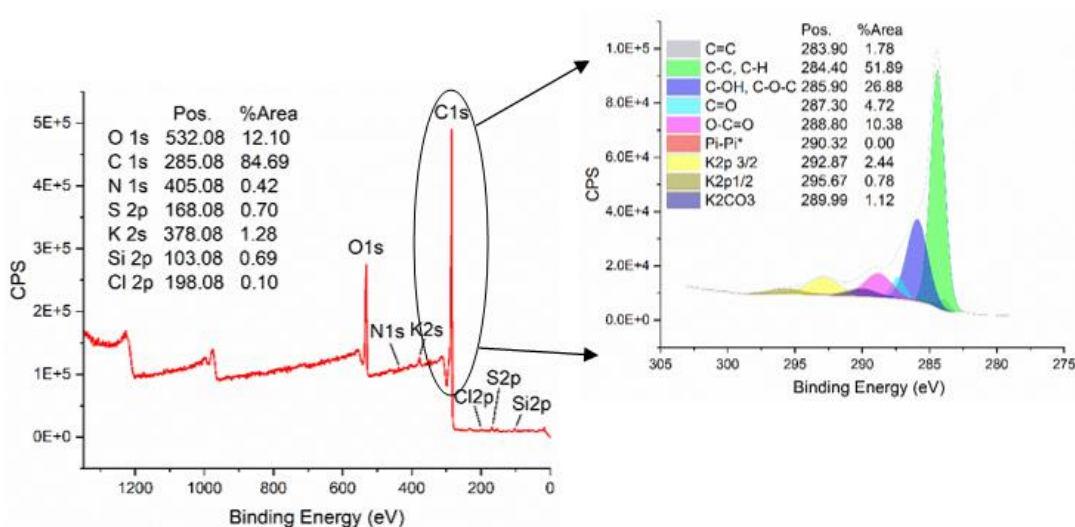


Figure 2.1: Survey scan showing relative elemental composition of an activated carbon surface (left). C1s and K2p high-resolution scan with synthetic component fitting of the same activated carbon surface (right).

The XPS analyses of all activated carbons were carried out using a Thermo Fisher Scientific K-Alpha spectrometer with a monochromatic Al K (alpha) source (15 mA, 15 kV). Survey scan analyses were conducted with an analysis area of 300 x 700 microns and a pass energy of 160 eV. High resolution analyses were carried out with an analysis area of 300 x 700 microns and a pass energy of 20 eV. Spectral processing and peak fitting were done using CASA XPS (version

2.31) with the binding energy spectra corrected to the main line of the carbon 1s spectrum at 284.85 eV.

2.1.3 Point of Zero Charge

The point of zero charge (PZC) is a surface charge parameter that provides insights into the charge density of a material's surface (Tran et al., 2017). It is equivalent to the pH at which a net neutral charge occurs for all surfaces of a material (both external and internal). This becomes very useful in predicting favorable and unfavorable interactions between charged species such as naphthenic acids and activated carbon. Thus, PZC is an important parameter to measure for all adsorbents used in this thesis.

The pH drift method was used to determine the PZC of each activated carbon (Ntakirutimana et al., 2019). Briefly, this included adjusting fixed volumes of a 0.01 M NaCl solution to pH levels from 2 to 12 with either dilute NaOH or HCl, followed by the addition of activated carbon that was then mixed for 24 hrs. The pH was

recorded before and after addition of activated carbon and used to estimate the PZC. Figure 2.2 provides an example of the data generated by this process.

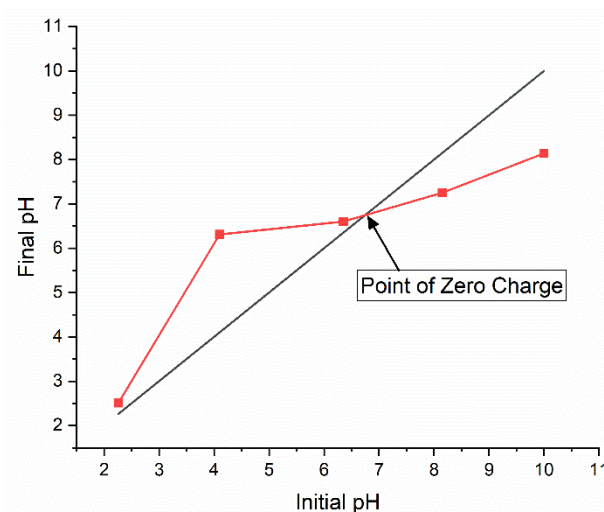


Figure 2.2: Point of zero charge calculation using the pH drift method. The intersection between the experimental pH drift (red line) and initial pH (black line) indicates charge neutrality.

2.2 Activated Carbon Synthesis

2.2.1 Petroleum Coke Activated Carbon

Petroleum coke from oil sands processing, as provided by Suncor Energy Inc. Calgary Alberta Canada, was used as the feedstock for the synthesis of several KOH activated carbons. A standard activated petroleum coke, abbreviated PAC, was produced as described by Strong et al and summarized here (Strong et al., 2023b). Petroleum coke was ground to particle sizes less than 0.308 mm, placed in a crucible and pretreated by heating the petroleum coke at 400 °C in a muffle furnace under air for 1 hour to remove any volatile compounds. Five grams of pretreated petroleum coke was mixed with dry KOH at a mass ratio of 1:1. Previous work in our laboratory had demonstrated that grinding the petroleum coke to 0.308 mm helped ensure a homogeneous mixture with KOH. The mixture was placed in crucibles and heated at 40 °C min⁻¹ to 410 °C under nitrogen (2L min⁻¹) and held for 30 minutes. The mixture was activated by continued heating of the sample under a nitrogen atmosphere at 90 °C min⁻¹ up to 900 °C, where it was held for 15 minutes.

Variants of PAC were also produced in which additional activation cycles were conducted on the unwashed PAC (Strong et al., 2023b). Briefly, following the first round of activation at 900 °C, samples were allowed to cool to room temperature and then were crushed and remixed followed by either 1 or 2 additional rounds of heating at 900 °C without any additional chemical inputs. Crushing/remixing the material was necessary since the unreacted KOH tends to separate out on top of the PAC. These additional activation cycles were used to convert microporosity to

mesoporosity without sacrificing specific surface area. All PAC adsorbents were washed with 20 mL of water per gram of unwashed activated product followed by vacuum filtration and dried at 110 °C.

2.2.2 Waste Wood Activated Carbon

Waste wood from construction sites in Ontario, underwent size reduction until the material could be passed through an 18 mesh sieve (less than 1.0 mm). A 1:1 dry mass ratio of 25% H_3PO_4 to waste wood was mixed and samples were digested for 20 hrs at 35 °C. The digested waste wood was placed in a muffle furnace for 30 minutes at 400 °C under a nitrogen flow of 5 L min⁻¹. These samples were ground and washed with 10 mL 0.1 M HCl to 1 g of the unwashed product at 80 °C for 1 hr with agitation, followed by 10 mL 0.1 M NaOH to 1 g unwashed product and finally 10 mL of DI water to 1 g unwashed product at 80 °C. Samples were dried at 110 °C overnight. To reduce oxygen functionality on the activated carbon, a final heat treatment step was carried out with 5 g of product heated to 900 °C for 15 minutes under N_2 . Following heat treatment, samples were washed and dried at 110 °C.

2.3 Batch Adsorption Techniques

2.3.1 Adsorption Kinetics

Adsorption is fundamentally a process that involves the uptake of an adsorbate onto the surface of an adsorbent until either saturation of the adsorbent surface or complete removal of the adsorbate from solution occurs. Initial rapid uptake of the adsorbate, followed by a continual deceleration, will proceed until an equilibrium between the occupation of adsorption sites within the adsorbent and

the remaining solution concentration of the adsorbate occurs. The adsorption kinetics are generally characterized by three main phases (Wang and Guo, 2020). First, external diffusion, from the bulk solution to the interface at the adsorbent's surface occurs, driven by the high concentration gradient present. This is followed by internal diffusion through the porous network of the adsorbent and finally concludes with the actual adsorption step onto vacant sites within the adsorbent. The adsorption step may be composed of a variety of mechanisms such as hydrogen bonding, electrostatic interactions, or chemical bond formation (Worch, 2012). A visual representation of the transportation of an adsorbate to vacant sites within a porous adsorbent is given in Figure 2.3.

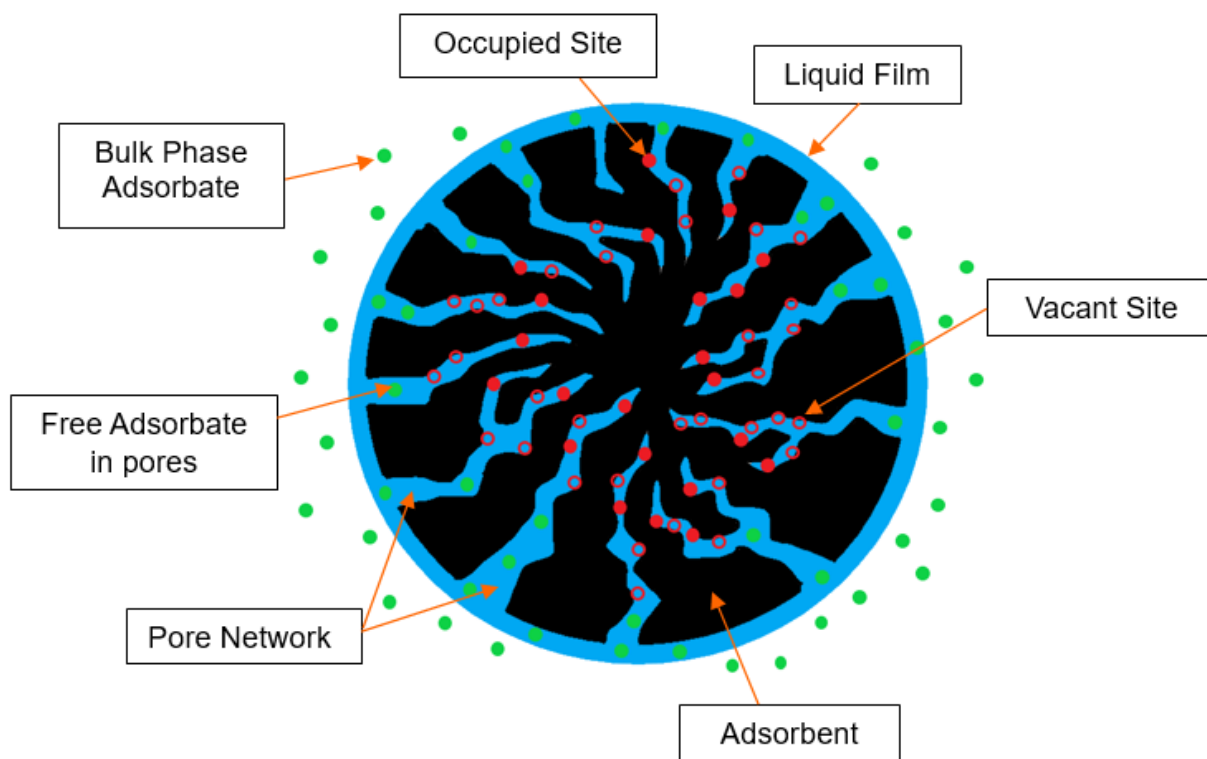


Figure 2.3: Schematic of adsorbate transportation through a porous adsorbent to adsorption sites.

As explained in Chapter 1, batch adsorption kinetic tests are often used to evaluate the time dependent adsorption behavior of solution-based species, while using EQ1, the material balance expression, to determine the adsorption capacities at each time point. For the kinetic evaluation of individual model naphthenic acids, an initial concentration of 40 mg L^{-1} was used for all kinetic experiments throughout this thesis, as this is within the range of concentration typically found within oil sands process affected water. A fixed mass of each adsorbent was evaluated up to either 48 or 72 hrs. Different mixing speeds ranging from 150 to 200 rpm were tested using a Thermo Scientific MaxQ 416 HP orbital shaker. All model naphthenic acid solutions were buffered to a pH of 8 using an inorganic phosphate buffer to simulate the pH of oil sands process water and all the time points were evaluated in triplicate by mixing 3 separate samples for each time point. $0.45 \mu\text{m}$ syringe filters were used to filter each batch sample so concentrations could be analyzed via TOC analysis. An example of the adsorption kinetics for diphenylacetic acid (DPA) onto phosphoric acid activated waste wood (HAC) is shown in Figure 2.4, in which q_e , the adsorption capacity in milligram of carbon adsorbed per gram of adsorbent (mg C g^{-1}) is graphed against mixing time.

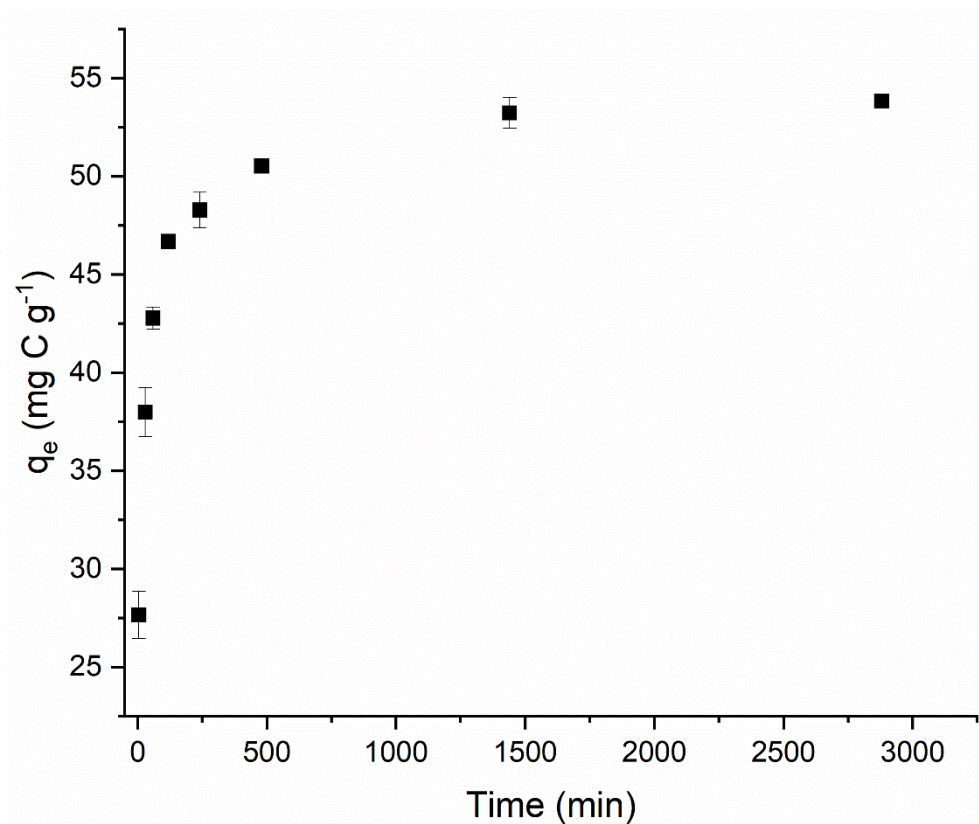


Figure 2.4: DPA adsorption kinetics on a phosphoric acid activated waste wood.

2.3.2 Adsorption Isotherms

Another highly useful batch adsorption test that typically accompanies a kinetic evaluation of an adsorbate's uptake onto an adsorbent is the adsorption isotherm. This test is specifically designed to evaluate how much of an adsorbate can be adsorbed, and thus is very useful in optimizing an adsorption system. Adsorption equilibrium is a dynamic process, that is dependent on both the amount of adsorbent exposed to an adsorbate solution and the concentration of that adsorbate. Modifying either of these parameters will cause a shift in the equilibrium established, which is the fundamental basis for adsorption isotherms. This allows for two main approaches when producing isotherms for model

naphthenic acids. Either a variable mass method, in which a range of adsorbent dosages are selected while maintaining a constant concentration of model naphthenic acids, or a variable concentration method, in which a constant mass of adsorbent is mixed with a range of initial concentrations of model naphthenic acids (Piccin et al., 2017). Both approaches are suitable to produce adsorption isotherms. These experiments generally require a reasonable amount of preliminary work involving optimization of each of these variables to achieve a complete isotherm.

A variable mass method was employed for all isotherms presented in this thesis, in which the proper dosage of each adsorbent used was carefully optimized to produce an isotherm based on a 60 mg L^{-1} initial concentration for each individual model naphthenic acid. This was done by initially testing the adsorption performance of a series of adsorbent dosages and then modifying the final range of dosages used based on the isotherms produced. 60 mg L^{-1} was chosen instead of 40 mg L^{-1} , as this was deemed a more optimal starting concentration that was conducive for producing a complete isotherm while still being within the range of naphthenic acids found in oil sands process affected waters. Depending on the adsorbent used, mixing times ranged from 24 to 72 hours to ensure equilibrium was achieved. All solutions and mass to volume ratios evaluated for a given isotherm were similarly buffered at a pH of 8 and tested in triplicate. Adsorption isotherms are expressed in terms of adsorption capacity at equilibrium, q_e , versus equilibrium concentration in solution, C_e . An

example adsorption isotherm for DPA using a KOH activated petroleum coke is presented in Figure 2.5.

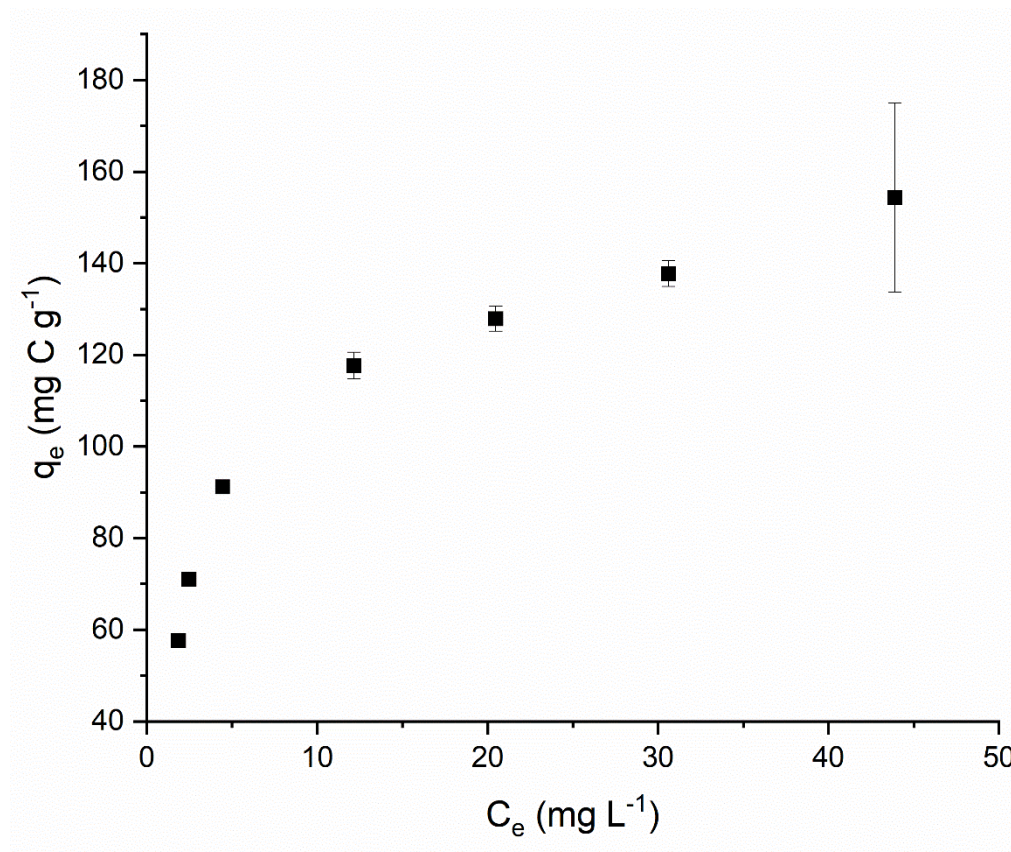


Figure 2.5: DPA adsorption isotherm on KOH activated petroleum coke.

2.4 Adsorption Kinetic Modelling

The modeling of adsorption kinetics provides details about the rate limiting steps, gives insights into the mechanisms of adsorption, and can be used to determine activation energies associated with the adsorbate/adsorbent interaction (Saha and Chowdhury, 2011; Wang and Guo, 2020). Kinetic modelling within this thesis primarily served to highlight differences between the uptake rates of model naphthenic acids onto different activated carbons and to estimate

adsorption activation energies. Numerous models have been proposed and utilized throughout the literature, like the commonly employed empirical pseudo first (PFO) and second order (PSO) kinetic models (Plazinski et al., 2013).

Although these models have been criticized for lacking any consistent physiochemical meaning (Tan and Hameed, 2017), they both present mathematical forms that adhere appreciably well to many adsorption systems. Within this thesis the usage of the PFO and PSO models was replaced with the multi-exponential model (m-exp) due to its superior fitting abilities.

2.4.1 Multi-exponential Model (m-exp)

The m-exp model has been regarded as a series of pseudo first order processes that work in parallel to fit experimentally determined adsorption kinetics (Marczewski et al., 2016).

$$q_t = a_e - a_e \sum_{i=1}^n f_i \exp(-k_i t) \quad \text{EQ5}$$

Where,

$$\sum_{i=1}^n f_i = 1$$

Here, f_i represents the fraction of the adsorption kinetics that is described by the rate constant k_i (min^{-1}). EQ5 was used strictly as an empirical expression to determine model independent half times of adsorption $t_{1/2}$ (min). The n value for EQ5 was determined based on an error analysis using several error functions of

different n values as described in section 2.6. These were used for comparison purposes between different model naphthenic acid adsorption systems, and to approximate activation energies for model naphthenic acid uptake as explained in Section 2.7.3.

2.5 Adsorption Isotherm Modelling

Adsorption isotherms are often accompanied by models used to describe the equilibrium behavior of the adsorption system. Different isotherm models are based on different assumptions about the adsorption system in question which can be used to gain insights into mechanistic aspects. Information on monolayer versus multilayer coverage of the adsorbent surface for instance may be postulated based on the models used. Isotherm modelling can be particularly useful when exploring thermodynamic parameters associated with adsorption. There are a considerable number of isotherm models used in adsorption literature, that often range from being semi empirical to empirical. Here, four commonly used models are presented that were used to describe model naphthenic acid adsorption systems.

2.5.1 Langmuir

Although first developed to explain gas phase adsorption, the Langmuir isotherm model has been extensively used to explain adsorption of aqueous systems (Foo and Hameed, 2010). The model makes very clear assumptions that adsorbed species form only a monolayer with no interactions with adjacent

adsorbed species and that the energy related to adsorption at each site on an adsorbents surface is constant, implying a homogeneous surface.

$$q_e = \frac{Q_0 K_L C_e}{1 + K_L C_e} \quad \text{EQ6}$$

In EQ6, Q_0 (mg g^{-1}) and K_L (L mg^{-1}) are representative of the monolayer saturation capacity and the Langmuir constant respectively. K_L is directly related to the adsorbate affinity to an adsorbents surface.

2.5.2 Freundlich

The empirical Freundlich isotherm model (EQ7) has been commonly used to represent adsorption onto activated carbon due to the typically heterogenous nature of the adsorbent's surface (Worch, 2012). It predicts an infinite increase in adsorption capacity with increasing equilibrium concentration, implying multilayer adsorption.

$$q_e = K_F C_e^{1/n} \quad \text{EQ7}$$

In EQ7, K_F ($(\text{mg g}^{-1})/(\text{L mg}^{-1})^{1/n}$) is the Freundlich constant describing the strength of adsorption, while $1/n$ is the heterogeneity factor in which values closer to zero indicate a more heterogeneous surface.

2.5.3 Redlich Peterson

While the Langmuir and Freundlich models are both commonly used, they can sometimes be insufficient to explain equilibrium behavior in adsorption systems.

The Redlich Peterson equation is a three parameter model that combines both the Langmuir and Freundlich expressions together (Piccin et al., 2017). Thus, making it a more flexible empirical expression.

$$q_e = \frac{K_R C_e}{1 + a_R C_e^g} \quad \text{EQ8}$$

Within EQ8, K_R (L g^{-1}) and a_R (L mg^{-1})^g are the Redlich Peterson constants respectively, while the parameter g represents the heterogeneity factor. The value of g is restricted to between 0 and 1. When the concentration of the adsorbate is sufficiently high, EQ8 reduces to the Freundlich expression, while at sufficiently low concentrations EQ8 will reduce to a linear isotherm (Henry's Law) (Eder et al., 2021).

2.5.4 Sips

The Sips expression is another empirical combination of the Langmuir and Freundlich models.

$$q_e = \frac{Q_{ms} K_s C_e^{\beta S}}{1 + K_s C_e^{\beta S}} \quad \text{EQ9}$$

In EQ9, Q_{ms} (mg g^{-1}) and K_s (L mg^{-1}) ^{βS} are the maximum monolayer saturation capacity and the Sips constant respectively, while βS is the heterogeneity factor. EQ9 reduces to the Langmuir model at sufficiently high adsorbate concentrations, thus predicting maximum surface coverage and reduces to the Freundlich model at low adsorbate concentrations.

2.6 Model Evaluation

Fitting analysis of adsorption kinetics and isotherm models were performed using a nonlinear least squares approximation in which the objective function, the sum of residuals squared, was minimized in accordance with the equation below.

$$SSR = \sum_i^n (q_{cal} - q_{exp})^2 \quad EQ10$$

Use of this equation involves an iterative process in which fitted values associated with a given model are changed to reduce the distance between calculated adsorption capacities, q_{cal} , and experimental q_{exp} using a suitable algorithm. All isotherm modelling and kinetic models using EQ10 were done with OriginPro Software (2022, version 9.9.0.225) using the Levenberg Marquardt algorithm.

Assessment of the kinetic and isotherm models used were evaluated through use of multiple error functions, as recommended by several authors (Foo and Hameed, 2010; Tran et al., 2017). The R^2 , adjusted R^2 , and reduced X^2 values were used for all modelling purposes while the corrected Akaike Information Criterion (AIC_c) was further used when comparing multiple isotherm models. A good description of using AIC_c values has been given elsewhere (Eder et al., 2021). Briefly, the lowest AIC_c value indicates the model that best represents the isotherm data relative to the other models. Comparison of AIC_c values often involves the use of EQ11:

$$\Delta_i = AIC_{c_i} - AIC_{c_{min}} \quad EQ11$$

Here, AIC_{cmin} is the isotherm model with the lowest AIC_c value, which when compared to the AIC_c values of other isotherm models provides an indication of whether other models suitably represent the isotherm data relative to the isotherm model with the minimum AIC_c .

2.7 Adsorption Thermodynamics

2.7.1 Standard State Thermodynamic Adsorption Parameters

Adsorption thermodynamics play a key role in characterizing an adsorption system and are vital for discerning the adsorption mechanism. The magnitude of the enthalpy change associated with adsorption can be used to distinguish between adsorption based on physical interactions (physisorption) and when chemical reactions involving bond formation occur (chemisorption) (Tran et al., 2017). This requires approximating standard state thermodynamic adsorption parameters. Several model naphthenic acid adsorption systems using PAC were evaluated using the van't Hoff expression.

$$\ln K_c = \frac{\Delta H^\circ}{R} * \frac{1}{T} + \frac{\Delta S^\circ}{R} \quad EQ12$$

EQ12 relates changes in temperature to the dimensionless equilibrium constant, K_c . Which allows standard state parameters of enthalpy ΔH° (kJ mol⁻¹), and entropy, ΔS° (J mol⁻¹ K⁻¹) to be determined from the slope and intercept of a linear plot respectively. Key to this method is the approximation of K_c , which has been shown to be applicable using certain isotherm models (Piccin et al., 2017).

K_c can be approximated using K_L taken from isotherm modelling using the Langmuir equation (EQ6). K_L , when in units of L mg⁻¹, can be shown to

theoretically relate to the equilibrium constant in EQ12 by use of EQ13 (Ghosal and Gupta, 2017; Liu, 2009).

$$K_c = \frac{K_L \left(\frac{L}{mg} \right) M_A \left(\frac{mg}{mol} \right)}{\gamma_e} C_r \left(\frac{mol}{L} \right) \quad EQ13$$

Where M_A is the molecular mass of the model naphthenic acid, while C_r and γ_e are the selected reference states (1 mol L^{-1}) and the activity coefficient (dimensionless) of the model naphthenic acid respectively. Selection of the standard reference state with conversion of K_L units into L mol^{-1} by use of the molecular mass of the model naphthenic acid, ensures a dimensionless K_c value in accordance with the dimensionality of K_c in EQ12. While γ_e for weakly ionizable species in solution, such as naphthenic acids, will decrease from unity with the increasing ionic strength of the solution. As described elsewhere, use of the Debye Huckel limiting law allows for an approximation of γ_e (Ghosal and Gupta, 2017). Thus, a series of adsorption isotherms were produced within a temperature range from 278 to 308 K, for individual model naphthenic acids and were modelled using the Langmuir approach. This was followed, using EQ12 and EQ13 to approximate standard state thermodynamic parameters. An environmental chamber was used to maintain a constant temperature of all isotherms produced.

In a second approach, using the Sips isotherm constant, K_s from EQ9, was also used to approximate K_c with similar considerations to obtain a dimensionless equilibrium constant (Tran et al., 2023).

$$K_c = \sqrt[\beta_s]{K_s} * M_A * \frac{C_r}{\gamma_e} \quad \text{EQ14}$$

2.7.2 Isosteric Enthalpy of Adsorption

The isosteric enthalpy of adsorption $\Delta_{ist}H$ is another thermodynamic property of adsorption systems that is useful to compare to ΔH° . It represents the ratio of infinitesimal change in heat exchanged over a comparable change in adsorbed amount. In contrast to ΔH° which is fundamentally based on an approximation of K_c that represents the entire experimental isotherm, $\Delta_{ist}H$ is produced for any individual data point on an adsorption isotherm. This approach provides a way to determine if the heat evolved during adsorption is a function of surface coverage (Nuhnen and Janiak, 2020). If an adsorbent with a homogeneous surface is used, $\Delta_{ist}H$ should remain constant regardless of surface coverage. When this occurs, $\Delta_{ist}H$ should be numerically equivalent to ΔH° . However, if $\Delta_{ist}H$ is shown to change as a function of surface coverage, ΔH° and $\Delta_{ist}H$ will not be equivalent. $\Delta_{ist}H$ can be calculated through use of the linear form of the Clausius Clapeyron equation (Salvestrini et al., 2014).

$$\ln C_e = \frac{\Delta_{ist}H}{R} \frac{1}{T} + \text{Con} \quad \text{EQ15}$$

In which a plot of $\ln C_e$ against $1/T$ should produce a straight line allowing for $\Delta_{ist}H$ (kJ mol⁻¹) to be determined from the slope. The same adsorption isotherms for model naphthenic acids conducted under a range of temperatures as described above, were used to evaluate $\Delta_{ist}H$. Values of C_e at a fixed q_e were

determined using the fitted parameters established from Langmuir modelling using the rearranged EQ16.

$$C_e = \frac{q_e}{Q_0 K_L - q_e K_L} \quad \text{EQ16}$$

2.7.3 Activation Energy

Activation energy E_a , is another thermodynamic property worth exploring in adsorption systems that can compliment standard state parameters. Activation energy is characterized as the minimum energy required for the adsorption interaction to occur in an adsorption system. A visual depiction is given in Figure 2.6. The magnitude of the activation energy can provide insights into the mechanism associated with adsorption. Similar to ΔH° , there is no strict range associated with different interaction mechanisms, but instead empirically approximated ranges associated with different types of interactions. For this reason, evaluation of several thermodynamic properties is beneficial to conclude the adsorption mechanism. For instance, activation energies below 40 kJ mol^{-1} are generally considered to be of physical means: van der Waal interactions, hydrogen bonding etc. Chemisorption is expected to yield activation energies above 40 kJ mol^{-1} . In contrast, ion exchange

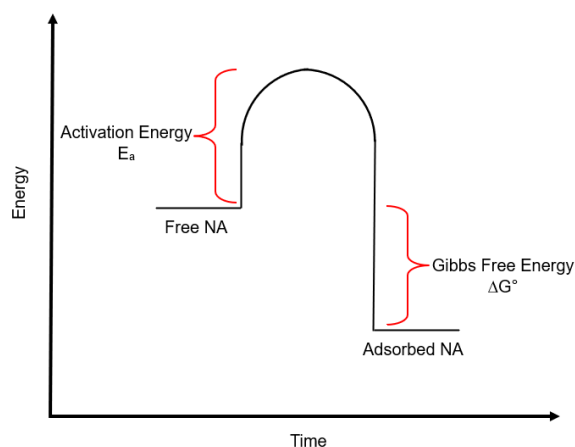


Figure 2.6: Energy diagram showing the relation of E_a to ΔG° for naphthenic acid (NA) adsorption.

processes have been shown to vary from 0.2 to 80 kJ mol⁻¹ (Inglezakis and Zorpas, 2012).

Activation energy can be calculated through use of the Arrhenius expression, which relates the rate constant of the adsorption system to temperature (Saha and Chowdhury, 2011). Since determining an intrinsic rate constant for adsorption systems is difficult with empirical kinetic models, an alternative approach using model independent half times of adsorption $t_{1/2}$ (min) was used instead of the rate constant (Marczewski et al., 2016). The time to reach 50% adsorption was determined through use of the m-exp model EQ5, which was applied to adsorption kinetics for several model naphthenic acids, evaluated within a temperature range from 278 to 308 K. Temperatures for these adsorption kinetics were controlled using an environmental chamber. Using the fitted parameters of EQ5, $t_{1/2}$ values for each adsorption kinetics were readily determined and could be used in accordance with EQ17 to approximate E_a .

$$\ln(t_{1/2}) = \ln A - \frac{E_a}{RT} \quad \text{EQ17}$$

Where, R is the gas constant (8.314 J mol⁻¹ K⁻¹). A plot of $\ln(t_{1/2})$ versus 1/T will yield a straight line in which E_a that can be determined from the slope of a linear regression.

2.8 Measurement Techniques

2.8.1 Total Organic Carbon (TOC) Analysis

TOC analysis is a commonly used instrumental technique for the determination of organic carbon content present in complex water sources. It is a

nonspecific technique that is incapable of differentiating between different organic species, but instead presents a lumped sum measurement of all organic species present. Thus, the technique has limited usefulness in characterizing OSPW, but given its simplicity, ease of operation, and universal detection of organic species, it can be useful when evaluating individual model naphthenic acids. This requires only a limited extent of method development and is well suited for evaluating the large volume of samples associated with the adsorption tests conducted on model naphthenic acids.

A Shimadzu TOC VCPH analyzer with an AIS-V autosampler was used to evaluate all model naphthenic acid adsorption tests (Shimadzu, 2010). This instrument functions by using a combustion chamber filled with a standard platinum catalyst set to 680 °C that is used to convert organic materials into CO₂. A filtered air carrier gas brings the sample to a non-dispersive near infrared detector (NDIR) that measures the CO₂ formed by the combustion. The system can operate in several different modes. For all model naphthenic acid species evaluated, a non-purgeable organic carbon (NPOC) method was used, which acidified samples, and was followed by a purging step, that used a carrier gas, to remove the inorganic carbon content. The sample was then injected into the combustion tube and analyzed, leading to an NPOC signal that is equivalent to the TOC signal. The only exception to this was analysis of dicyclohexylacetic acid (DCH), that required using a TC/IC method, in which the total carbon (TC) in the sample (which includes both organic and inorganic sources) was first measured followed by a measurement of inorganic carbon (IC). TC is measured simply

without an acidification and purging step, while IC is measured through use of a separate IC reaction vessel. A solution of phosphoric acid in the IC reaction vessel converts the inorganic carbon in the sample into CO₂ which is then carried to the NDIR detector. Simple subtraction of the IC from the TC measurements yields the final TOC concentration. When specified, external standards for model naphthenic acids were prepared and used to determine model naphthenic acid concentrations in adsorption samples.

3 Adsorption Kinetics of Model Naphthenic Acids

3.1 Introduction

A fundamental aspect of adsorption science is the characterization of the time dependent evolution of adsorbate transfer to an adsorbents surface. It often serves as a preliminary tool to determine the equilibration time necessary to explore the adsorption isotherm. Optimization of the uptake kinetics are, however, equally as important as equilibrium studies, because of the often, time sensitive nature of adsorbent application. The adsorption of naphthenic acids is no exception to this, as a likely approach will involve utilizing a piping system in which activated carbon will have a limited contact time with the oil sands process affected water (OPSW) that it aims to treat. Thus, understanding the physical properties of porous adsorbents that give rise to suitably fast kinetics is a vital endeavor necessary to explore and will additionally serve to establish the required mixing conditions for equilibrium studies.

Given the complexity of the naphthenic acid fraction present in OSPW, a series of individual model naphthenic acid species were used to survey their uptake kinetics onto activated carbon. Several candidate adsorbents were explored to both evaluate how variable naphthenic acid uptake rates might be and to determine which adsorbent properties should be optimized. It has been consistently shown that adsorption kinetics of various contaminants onto porous materials is heavily influenced by pore development. Mesoporosity (2 to 50 nm) in particular, is especially influential towards achieving faster adsorption kinetics, as larger more opened porosity allows for faster internal mass transfer, greatly

improving the overall kinetic process (Ighalo et al., 2021; Suresh Kumar et al., 2019). Adsorption kinetics have often been shown to change as a function of particle size as well, as smaller particle sizes usually offer reduced internal resistance to diffusion (Kang et al., 2018; Suresh Kumar et al., 2019). Only limited information on the kinetic behavior of model naphthenic acids is currently available in the adsorption literature. Of the few adsorption studies involving porous adsorbents and model naphthenic acids, there is usually a larger focus on demonstrating high adsorption capacities with less focus on kinetics (Martinez-Iglesias et al., 2015; Niasar et al., 2016). Thus, given its importance, a detailed evaluation of the effects of pore size and particle size distribution on adsorption kinetics of model naphthenic acids is presented below.

3.2 Materials & Methods

Diphenylacetic acid (DPA) (CAS# 117-34-0), dicyclohexylacetic acid (DCH) (CAS# 52034-92-1), cyclohexane acetic acid (CHA) (CAS# 5292-21-7), 2-methyl-1-cyclohexanecarboxylic acid (MCH) (CAS# 56586-13-1), 1,4-cyclohexanedicarboxylic acid (DCA) (CAS# 1076-97-7), heptanoic acid (HA) (CAS# 111-14-8), and succinic acid (SA) (CAS# 110-15-6) were all purchased from Sigma Aldrich (St. Louis, MO). The commercial activated carbon (CAC) used was purchased from Strem Chemicals. While all petroleum coke and wood waste derived adsorbents mentioned followed activation procedures given in Chapter 2 section 2.2. Size fractionation described in this chapter used a size fractioning device with set mesh sizes that could separate and allow for a particle

size distribution to be determined. All adsorption experiments presented here followed the procedure provided in Chapter 2 section 2.3.1.

3.3 Adsorption Kinetics on Physically Different Activated Carbon

3.3.1 Surface Characteristics of each Adsorbent

The adsorbents used to evaluate uptake kinetics of model naphthenic acids were characterized through several different techniques. Most notably, these included BET surface area analysis and particle size distribution. Table 3.1 includes a complete breakdown of the specific surface area and pore size distribution of each activated carbon. The petroleum coke derived activated carbon (PAC) exhibited the lowest specific surface area and largest extent of microporosity as evident by the micropore volume. While both the heat-treated phosphoric acid activated waste wood (HAC) and CAC had a similar surface area but differing extents of micro and mesoporosity. This gave rise to three different activated carbons that had considerably different pore size distributions, in which the PAC was nearly 80% microporous, while in contrast HAC was only 25% microporous and CAC contained nearly equal amounts of micro and mesoporosity.

Table 3.1: BET surface area analysis of activated carbon adsorbents used.

Adsorbent	Specific Surface Area ($\text{m}^2 \text{g}^{-1}$)	Total Pore Volume ($\text{cm}^3 \text{g}^{-1}$)	Micropore Volume ($\text{cm}^3 \text{g}^{-1}$)	Mesopore Volume ($\text{cm}^3 \text{g}^{-1}$)
PAC	956 ± 34	$0.402 \pm 1.3 \times 10^{-2}$	$0.322 \pm 1.2 \times 10^{-2}$	$0.080 \pm 7.0 \times 10^{-2}$
HAC	1440 ± 78	$0.761 \pm 1.5 \times 10^{-2}$	$0.190 \pm 6.7 \times 10^{-3}$	$0.572 \pm 2.2 \times 10^{-2}$
CAC	1310 ± 69	$0.476 \pm 1.0 \times 10^{-2}$	$0.261 \pm 1.6 \times 10^{-3}$	$0.215 \pm 1.2 \times 10^{-2}$

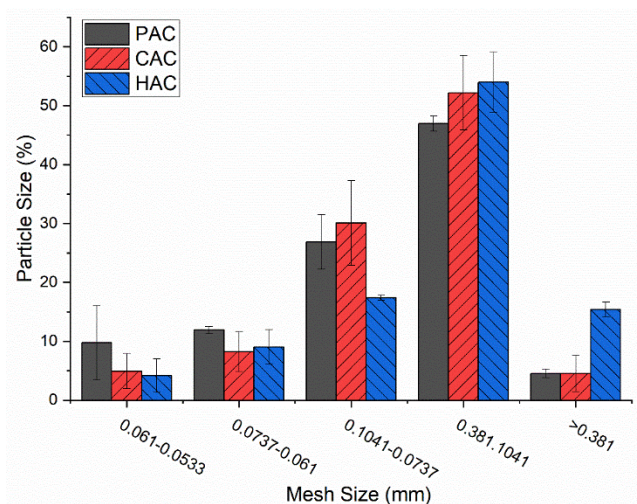


Figure 3.1: Particle size distribution of each activated carbon.

The particle size distribution also varied between each activated carbon. The most notable difference was the larger extent of the greatest particle size fraction of > 0.381 mm diameter particles observed for HAC as seen in

Figure 3.1. This was also apparent upon visual assessment of HAC.

In contrast, both PAC and CAC clearly shared a more similar profile.

3.3.2 Adsorption Kinetics on each Activated Carbon

Adsorption kinetics of 7 model naphthenic acid species were evaluated with respect to PAC, HAC, and CAC as shown in Figure 3.2. Regardless of the adsorbent used, the adsorption capacities obtained by 48 hrs of mixing clearly varied considerably amongst each model naphthenic acid. Although interesting to note, the exact reasons for this variability are explored in more detail in chapters 4 and 5 that pertain to adsorption isotherms. More importantly, the uptake kinetics on each activated carbon was clearly different. This is most obvious when comparing the kinetics of CAC and PAC. Adsorption equilibrium for most model naphthenic acids was achieved approximately within 60 minutes on CAC, while equilibrium on PAC varied between 24 to 48 hrs.

These differences in kinetics were further explored through kinetic modelling using the m-exp model (EQ5) to estimate half times of adsorption ($t_{1/2}$). Figure

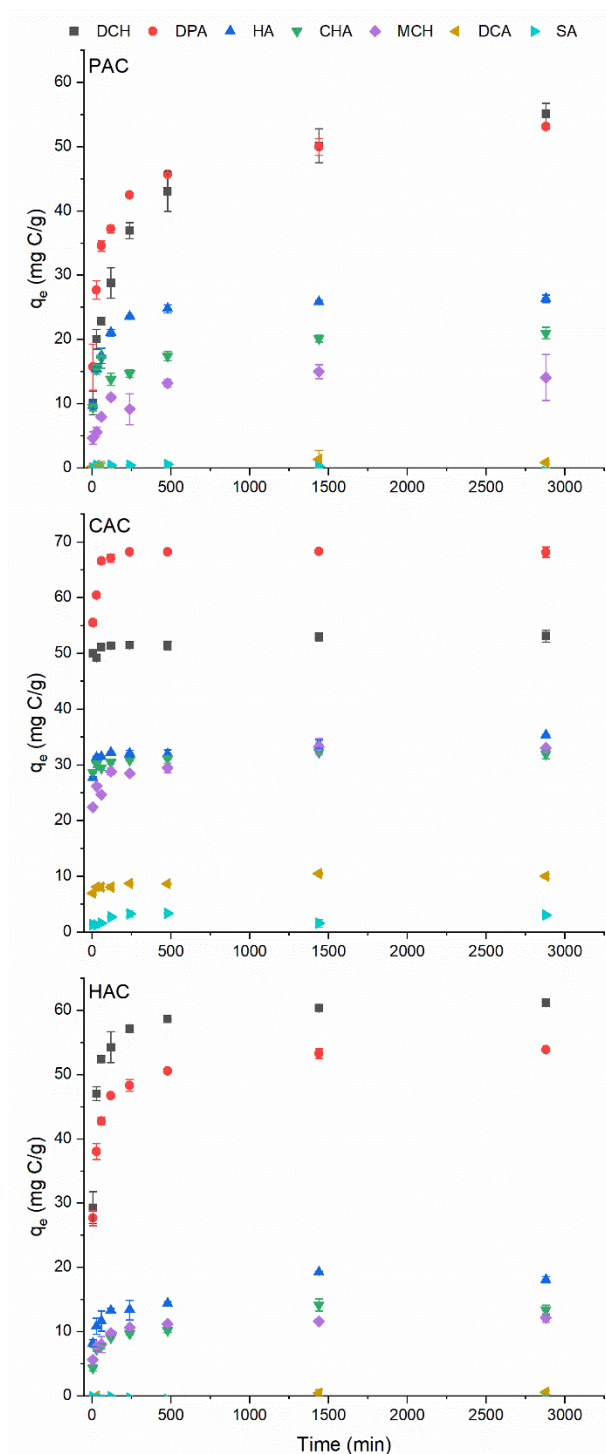


Figure 3.2: Uptake kinetics of model NAs onto each activated carbon.

3.3 shows the m-exp model fit for the uptake kinetics of 5 model naphthenic acids onto both PAC and HAC. Succinic acid (SA) and 1,4 cyclohexanedicarboxylic acid (DCA) were excluded from m-exp modelling since little to no adsorption was observed in Figure 3.2. Additionally, the adsorption kinetics on CAC were not modelled well by the m-exp model, regardless of how many fitting parameters were used. k_i and f_i fitting parameters ranging from just using k_1 and f_1 or up to k_3 and f_3 were explored for kinetic modelling on CAC. The poor fitting performance is most likely a result of uptake of each model naphthenic acid onto CAC occurring very rapidly in which nearly all experimental data points are near or at the adsorption equilibrium for that respective model

species. Modelling of adsorption kinetics should ideally have experimental data points representative of the complete time evolution of the kinetic process for

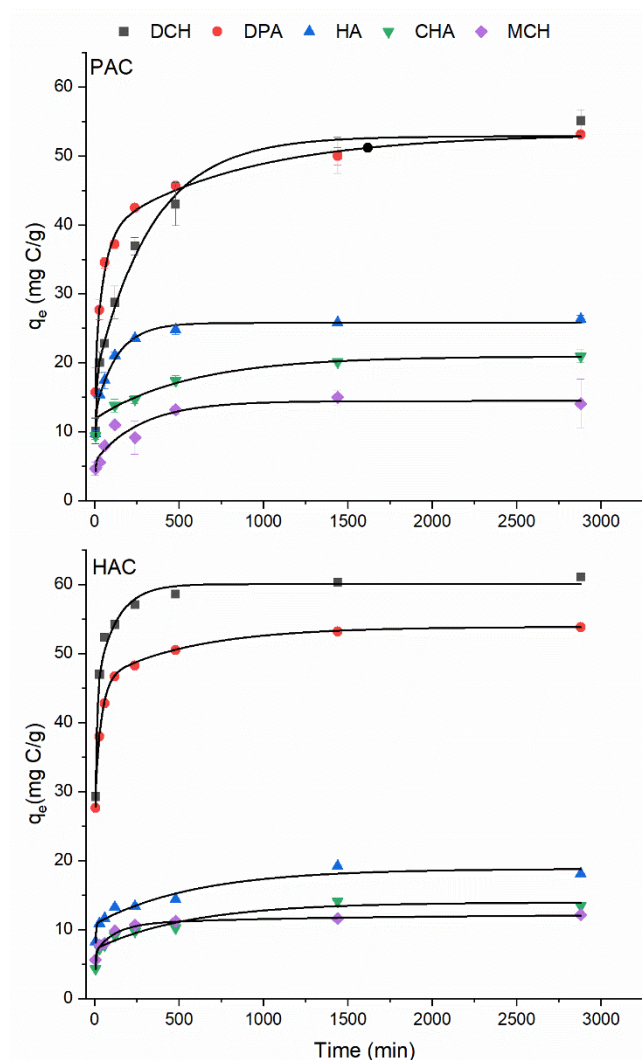


Figure 3.3: Kinetic modelling using $m\text{-exp}$ for each model NA onto PAC and HAC.

adequate model fitting (Tran et al., 2017). For instance, the $t_{1/2}$ value for each model naphthenic acid onto CAC was well within 5 minutes of mixing, meaning that 7 out of the 8 time points evaluated were near or at equilibrium. For the model species that could suitably be represented by EQ5, $t_{1/2}$ values were estimated and are shown in Table 3.2. In general, $t_{1/2}$ values were the longest on the PAC in comparison to HAC, while $t_{1/2}$ values on CAC were the shortest.

The differences in adsorption kinetics between each activated carbon are predominately caused by differences in their respective pore size and particle size distributions. As shown in Table 3.1, CAC, and HAC both have much greater mesopore volume compared to the mesoporosity of PAC, which should lead to faster kinetics on these two adsorbents. This is because, mesoporosity is much better suited to facilitate

internal diffusion of adsorbates in comparison to microporosity. Although both CAC and PAC maintained a similar distribution of particle sizes, there is a notable increase in the largest size fraction for HAC. Larger particle sizes tend to reduce adsorption kinetics (Kang et al., 2018; Suresh Kumar et al., 2019). The increased particle size observed with HAC likely explains why adsorption kinetics on this adsorbent are slightly slower than on the CAC despite the HAC having the largest volume of mesoporosity. Adsorption kinetics for any of these adsorbents could thus be further optimized by modification of either particle size or pore size distribution.

*Table 3.2: Adsorption half times for model naphthenic acids onto each activated carbon based on m-exp modelling, along with fitting analysis. *CAC was not modelled by m-exp, and thus adsorption half times are direct approximations from experimental adsorption kinetics.*

	HAC			PAC			*CAC
Model NA	$t_{1/2}$ (min)	R ²	Reduced X ²	$t_{1/2}$ (min)	R ²	Reduced X ²	$t_{1/2}$ (min)
DCH	6	0.9883	8.969	98	0.9914	4.893	< 5
DPA	4	0.9977	1.237	24	0.9960	4.581	< 5
HA	7	0.9621	1.169	11	0.9952	0.3866	< 5
CHA	16	0.9725	0.6607	7	0.9976	0.6319	< 5
MCH	7	0.9883	0.4222	53	0.9089	3.203	< 5

3.4 Impact of Adsorbent Physical Properties on Model Naphthenic Acid Uptake

3.4.1 Effect of Particle Size on Naphthenic Acid Adsorption Kinetics

The impact of particle size on uptake kinetics of model naphthenic acids was explored further. An alternative KOH activated petroleum coke, abbreviated here as PACV2 was used. This adsorbent was size fractioned into two main particle sizes of 0.1041 to 0.38 mm and < 0.1041 mm, while a portion of the original PACV2 without any size fractioning was kept for comparison. Interestingly, BET

surface area analysis in Table 3.3, showed a considerable difference in specific surface area and pore size distribution of PACV2 depending on the size fraction analyzed. The < 0.1041 mm size fraction had a larger surface area and mesopore percent in comparison to the 0.1041 to 0.38 mm size fraction. While the original unsized PACV2 clearly obtained surface area properties in between that of the two size fractions. The Table 3.3 results, highlight how variable the surface area properties are depending on the particle size isolated. These pronounced differences seen in Table 3.3 are likely a reflection of differences in pore development that persist during the activation stage for the petroleum coke precursor (Bagheri and Abedi, 2009).

Table 3.3: BET surface area analysis of PACV2.

Size Fraction	<0.1041mm	0.1041-0.38mm	unsized
Specific Surface area ($\text{m}^2 \text{g}^{-1}$)	1380	817	1030
Total Pore volume ($\text{cm}^3 \text{g}^{-1}$)	0.700	0.380	0.501
Micropore Volume ($\text{cm}^3 \text{g}^{-1}$)	0.283	0.224	0.248
Micropore (%)	40.4	59.3	49.6
Mesopore (%)	59.6	40.7	50.4

As shown previously in Figure 3.1, a significant fraction of the particle size distribution of the PAC adsorbent is much larger than 0.1041 mm, implying that a significant loss of product would ensue if the more optimal particle size of < 0.1041 mm was isolated for use after production. This may point to a need to better optimize the activation protocol to achieve a product with a more homogeneous particle size and pore size distribution. This is made clearer when

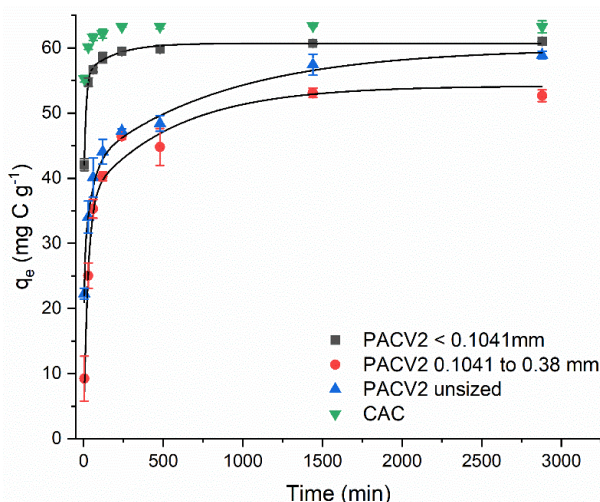


Figure 3.4: Adsorption kinetics of DPA onto PACV2 with m-exp modelling. Adsorption kinetics for DPA onto CAC is shown for comparison.

considering Figure 3.4 in which diphenylacetic acid (DPA) was used to evaluate uptake kinetics onto the PACV2 size fractions and Table 3.4 which shows $t_{1/2}$ based on m-exp modelling. Clearly adsorption kinetics are superior on the < 0.1041 mm size fraction in comparison to the 0.1041 to 0.38

mm size fraction. Unsurprisingly, the original PACV2 without sizing obtained a kinetics curve in between the two size fractions which agrees with the surface area properties displayed in Table 3.4. Figure 3.4 and Table 3.4 further exemplifies the need to ensure adsorbents used to treat naphthenic acids have a sufficient extent of mesoporosity to achieve fast kinetics, whether smaller particle sizes are used. Achieving lower particle sizes may also help improve adsorption capacity as implied by the significant increase in specific surface area and higher adsorption capacity obtained in Figure 3.4 for DPA on the < 0.1041 mm size fraction. However, this would need to be tested more thoroughly through adsorption isotherms of model naphthenic acids onto different size fractions.

Table 3.4: Adsorption half times ($t_{1/2}$) for DPA onto different size fractions of PACV2 based on m -exp modelling along with fitting analysis. Approximate $t_{1/2}$ for DPA onto CAC is included for comparison.

Adsorbent	$t_{1/2}$ (min)	R^2	Reduced X^2
< 0.1041 mm	< 5	0.9977	0.6233
0.1041-0.38 mm	33	0.9820	28.19
Unsize	14	0.9913	8.881
CAC	< 5	NA	NA

3.4.2 Effect of Pore Size Distribution on Naphthenic Acid Adsorption Kinetics

Physically modifying PAC to increase mesoporosity instead of isolating smaller particle sizes presents an alternative approach to ensure optimal kinetic conditions for the adsorption of naphthenic acids. This involved using a heat cycling procedure in which a petroleum coke/KOH mixture was subjected to several rounds of activation without any additional chemical inputs, causing progressive increases in mesoporosity with minimal changes to specific surface

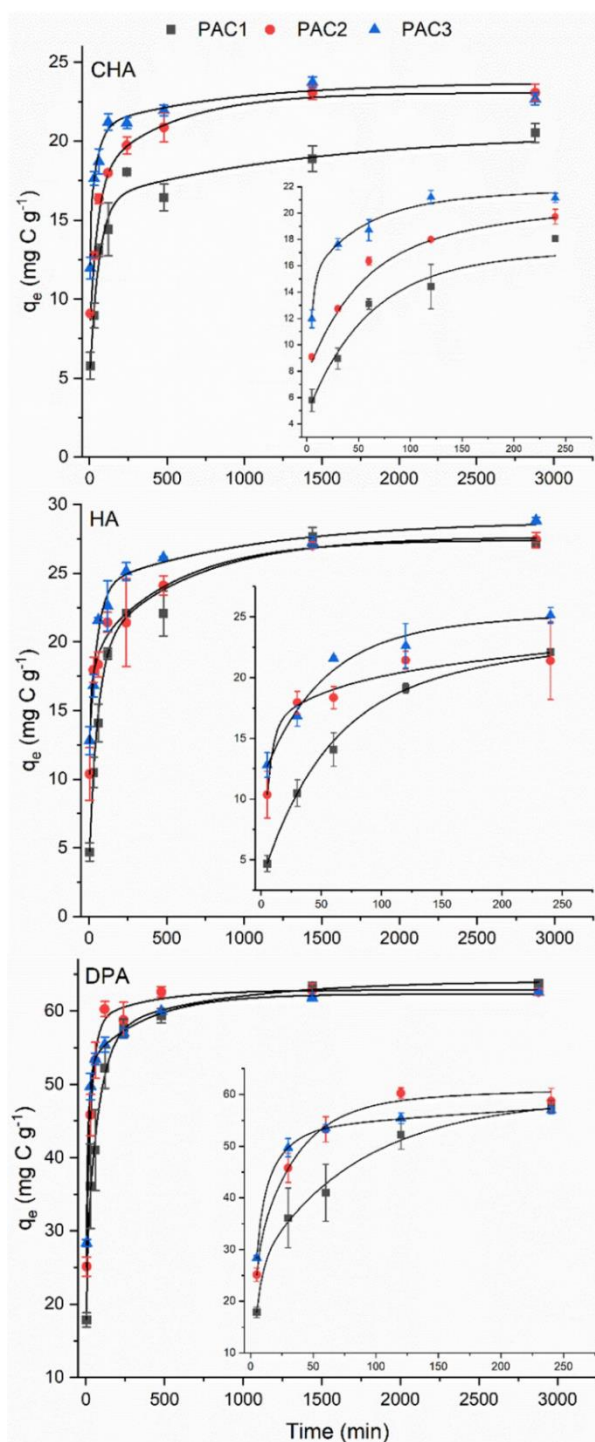


Figure 3.5: Adsorption kinetics of model naphthenic acids onto heat cycled petroleum coke derived activated carbon with m-exp modelling.

area (Strong et al., 2023b). A more detailed activation procedure is presented in Chapter 2 section 2.2.1. A 1:1 KOH to petroleum coke activated carbon was subjected up to 2 consecutive heat cycles, abbreviated here as PAC1 (no additional heat cycling), PAC2 (1 additional heat cycle), and PAC3 (2 additional heat cycles). Table 3.5 clearly displays the increase in mesoporosity that is seen while still maintaining appreciable yields. Model naphthenic acids were once again used to evaluate the kinetic uptake performance. As displayed in Figure 3.5, adsorption kinetics of cyclohexaneacetic acid (CHA), heptanoic acid (HA), and DPA were obtained on all three heat cycled

PAC products. Subsequent m-exp modelling was again used to

approximate $t_{1/2}$ for comparison of uptake rates. As seen in **Error! Reference**

source not found., adsorption half times consistently decreased with increasing heat cycling which is consistent with the increase in mesoporosity observed in Table 3.5. A minor exception to this was observed in the case of HA adsorption half time values in the PAC2 versus PAC3. However, a significant reduction in adsorption half time PAC1 versus PAC2 was still clearly observed for heptanoic acid. Noteworthy, is the fact that the surface chemistry of all three heat cycled products remained unchanged, based on XPS analysis which indicated negligible changes to the carbon and oxygen speciation present on the surface of these adsorbents(Strong et al., 2023b). These reductions in adsorption half times are a strong demonstration of how the increase in mesoporosity, achieved with multiple heating cycles, improves the adsorption kinetics.

Table 3.5: BET surface area analysis of heat cycled petroleum coke derived activated carbons. PAC1 was not subjected to any additional heat cycles after activation, PAC2 was subjected to 1 addition cycle, and PAC3 was subjected to 2 additional cycles.

Adsorbent	Specific Surface Area (m ² g ⁻¹)	Micropore Volume (cm ³ g ⁻¹)	Mesopore Volume (cm ³ g ⁻¹)	Micropore (%)	Mesopore (%)
PAC1	1059 ± 75	0.3438 ± 0.0260	0.1077 ± 0.0045	76.1 ± 0.61	23.9 ± 0.61
PAC2	1103 ± 37	0.3059 ± 0.0105	0.1984 ± 0.0077	60.7 ± 0.29	39.3 ± 0.29
PAC3	986 ± 27	0.1882 ± 0.0044	0.3277 ± 0.0231	36.5 ± 2.12	63.5 ± 2.12

Table 3.6: Adsorption half times for model naphthenic acids onto heat cycled petroleum coke derived activated carbon with fitting analysis for the m-exp model.

DPA	$t_{\frac{1}{2}}$ (min)	R ²	X ²
PAC1	20	0.9922	0.399
PAC2	8.4	0.9959	0.122
PAC3	6.6	0.9996	0.008
CHA	$t_{\frac{1}{2}}$ (min)	R ²	X ²
PAC1	34.3	0.9761	0.292
PAC2	18.5	0.9984	0.034
PAC3	4.5	0.9946	0.108
HA	$t_{\frac{1}{2}}$ (min)	R ²	X ²
PAC1	51.4	0.9915	0.184
PAC2	8.7	0.9941	0.116
PAC3	12	0.9956	0.109

3.5 Conclusion

Optimization of the physical characteristics, of low cost activated carbon adsorbents to achieve fast uptake rates, is an essential component for evaluation of naphthenic acid adsorption. Adsorption kinetics, of a series of model naphthenic acids, on several high surface area adsorbents, were presented in this chapter to survey differences between activated carbons with variable physical properties. Evidence is clearly presented on the importance of particle size and in particular pore size distribution towards obtaining appreciable adsorption kinetics of model naphthenic acids which was further supported by kinetic modelling.

4 Adsorption Isotherms of Model Naphthenic Acids

4.1 Introduction

Activated carbon has drawn attention as an effective adsorbent for treating process waters, due to the high surface areas achievable and low-cost feedstocks available (Martinez-Iglesias et al., 2015; Niasar et al., 2019). Studies have often demonstrated excellent uptake capacities, as high as 400 mg g⁻¹, for select model naphthenic acid species. Achieving high uptake capacities is an extremely desirable feature for an adsorbent, as it indicates that relatively low amounts of an adsorbent are needed to physically remove a contaminant from that source. However, the current available model naphthenic acid adsorption studies lack a more detailed exploration of how the adsorption process occurs, or whether high capacities are to be expected of all naphthenic acids within oil sands process affected water (OSPW). Research involving OSPW treatment with activated carbon has shown that for fixed hydrogen deficiency numbers (z) and increasing carbon numbers (n) naphthenic acids exhibit increased affinity towards activated carbon. This provides insights into the uptake affinity differences that exist between structurally different species (Islam et al., 2018). These results imply that some naphthenic acid species will be more resistant to adsorption on activated carbon than others. The now common approach of characterizing the naphthenic acid distribution, in terms of carbon and hydrogen deficiency, is limited in describing more specific structural features of these species due to the challenges of delineating all the contributing isomers for each set of n and z values (Brown and Ulrich, 2015).

The evaluation of individual surrogate naphthenic acid species offers a way to investigate the adsorption performance of specific naphthenic acid structures more thoroughly. With a considerable degree of structural diversity within the naphthenic acid distribution in OSPW, it is not surprising that there is variability in the physicochemical properties of naphthenic acids as well. Identifying whether certain naphthenic acid properties influence uptake affinity onto activated carbon is an important step towards predicting recalcitrant species. Understanding what physiochemical properties of organic contaminants influence adsorption for predictive purposes has been of interest in previous studies that have compared adsorption performance to key properties of adsorbates such as hydrophobicity (de Ridder et al., 2010). This can be achieved through an evaluation of the adsorption equilibrium, or adsorption isotherm, for model naphthenic acids. Subsequent modelling of adsorption isotherms is also often recognized as a critical step in optimizing an adsorption material and can provide some insights into the adsorption behavior (Piccin et al., 2017). In this work the commonly used isotherm models Langmuir, Freundlich, Redlich Peterson, and Sips were used to evaluate differences in adsorption performance between different naphthenic acid species.

By evaluating the adsorption performance on several different activated carbons with contrasting surface properties, favorable and unfavorable interactions could be identified, leading to an improved understanding of the adsorption mechanism. The same low-cost petroleum coke and waste wood based activated carbons presented in Chapter 3 are further explored here. The

model naphthenic acids chosen were composed of both aliphatic and cyclical species with single and double ringed structures that are known to exist in OSPW(Headley et al., 2016). Species with multiple carboxylic groups and some alkyl branching were also explored. These structural differences were chosen to expand upon the current research on model naphthenic acid adsorption present in the available literature.

4.2 Methods & Materials

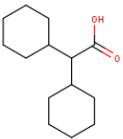
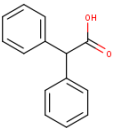

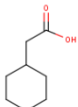
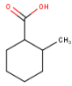
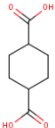
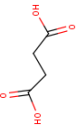
The same model naphthenic acids presented in Chapter 3 section 3.2 were utilized here, as well as the petroleum coke based activated carbon (PAC), phosphoric acid activated waste wood (HAC) and the commercial activated carbon (CAC). These adsorbents were characterized via XPS analysis to determine surface functionality in accordance with the method described in Chapter 2 section 2.1.2. Adsorption isotherm experiments followed the procedure outlined in Chapter 2 section 2.3.2.

4.2.1 Linear Modelling with Physicochemical Properties

A series of linear models were produced to test correlations between certain physicochemical properties of the model naphthenic acids against adsorption performance. This was done to explore whether certain properties of the model naphthenic acids were influencing adsorption. An approach described in Ridder *et al* was employed, in which the best representative isotherm model for each adsorption isotherm, on a given activated carbon, was used to predict adsorption capacity at a fixed C_e of 40 mg L⁻¹ (de Ridder et al., 2010). The C_e of 40 mg L⁻¹

was chosen since this value was in the experimental range of most model naphthenic acid adsorption isotherms. The Marvin Sketch software (ChemAxon) was used to approximate the physicochemical properties of the pKa and the pH dependent distribution coefficient (logD), which are displayed in Table 4.1. Linear correlations between the logarithm of the predicted adsorption capacity at C_e 40 mg L⁻¹ were tested against model naphthenic acid predicted properties for each activated carbon.

Table 4.1: Model naphthenic acids used along with predicted physicochemical properties.

	DCH	DPA	HA	CHA	MCH	DCA	SA
Structure							
pKa (predicted)	4.98	4.43	5.15	4.94	4.89	4.65 and 3.90	3.55 and 5.69
logD (predicted)	1.32	0.04	-0.51	-0.86	-0.79	-5.48	-6.17

DCH: Dicyclohexylacetic acid, DPA: Diphenylacetic acid, HA: Heptanoic acid, CHA: Cyclohexane acetic acid, MCH: 2-methyl-1-cyclohexanecarboxylic acid, DCA: 1,4-cyclohexanedicarboxylic acid, SA: and Succinic acid.

4.3 Characterization of Activated Carbons

4.3.1 XPS Surface Functionality

Table 4.2: Superficial atomic % composition by XPS and point of zero (PZC).

Adsorbent	C (%)	O (%)	N (%)	P (%)	K (%)	S (%)	PZC
PAC	85.5 ± 3.73	12.1 ± 2.31	0.4 ± 0.12	/	1.3 ± 0.53	0.6 ± 0.1	6.5
HAC	93.8 ± 1.41	5.3 ± 1.08	0.30 ± 0.30	0.6 ± 0.09	/	/	4.0
CAC	84.5 ± 1.68	15.5 ± 1.68	/	/	/	/	9.0

XPS survey scans for PAC, HAC, and CAC are shown in Table 4.2. The atomic percent of all three activated carbons were predominately composed of carbon and oxygen. Residual amounts of potassium in the form of potassium carbonate, left over from the KOH activation process, along with sulphur impurities were present in the final product of the PAC. Leaching tests on both PAC and HAC were evaluated using NPOC analysis demonstrating that no unstable organic carbon was removed from these adsorbents. In contrast to the surface of PAC, the CAC was clearly composed of a cleaner surface with no detectable impurities. The HAC contained a small atomic percentage of phosphorus, present in the form of phosphates or pyrophosphates, as indicated

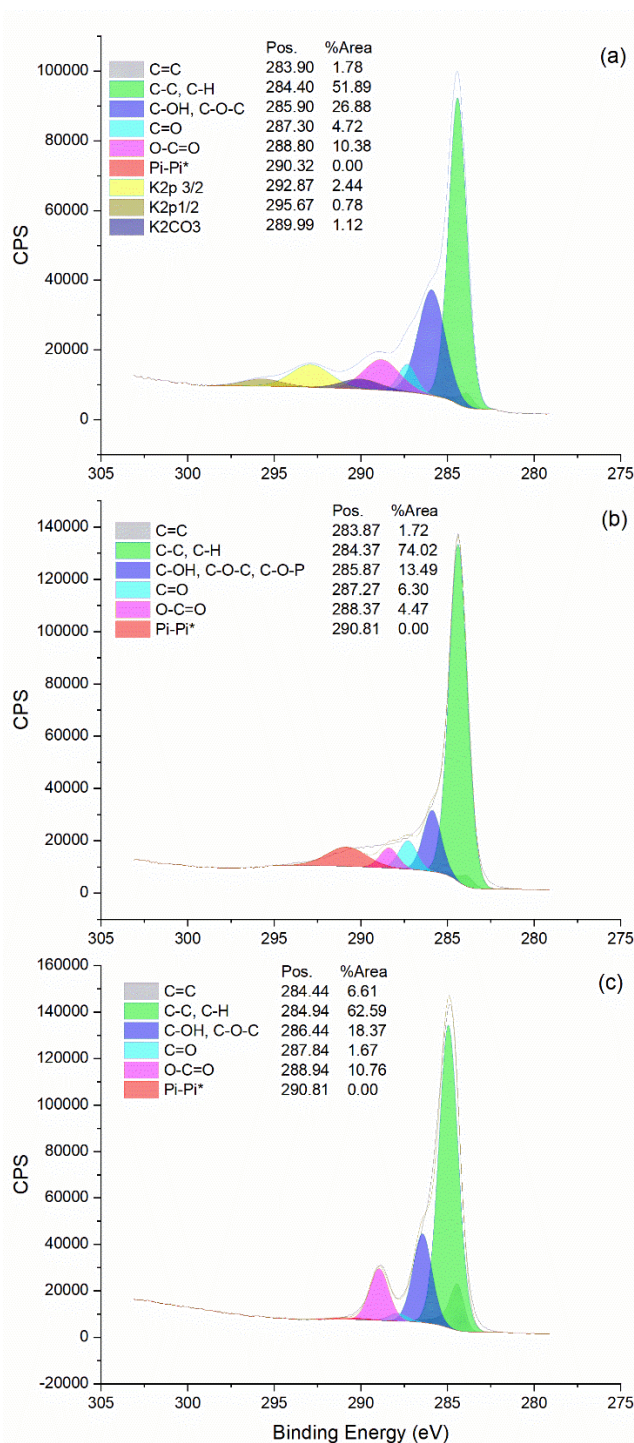


Figure 4.1: C1s scans for (a) PAC, (b) HAC, and for (c) CAC.

by the HAC high resolution P 2p scan included in Figure A.1.

Although similar types of oxygenated carbon species are present in the C 1s XPS region for all three activated carbons (Figure 4.1), a smaller atomic percent of oxygen is observed in Table 4.2 for the HAC in comparison to the other two activated carbons.

Additionally, clear differences in surface charge are expected due to the differences in point of zero charge (PZC) as seen in Table 4.2. XPS analysis clearly demonstrates distinct differences in the surface functionality of these three activated carbons, that should result in differences in adsorption capacities.

4.4 Adsorption Isotherms

As shown in the adsorption isotherms in Figure 4.2, adsorption performance is highly dependent on the individual naphthenic acids. High adsorption capacities in the range of 100 to 350 mg g⁻¹ were obtained for dicyclohexylacetic acid, (DCH), and diphenylacetic acid, (DPA), while adsorption capacities as low as 2 to 14 mg g⁻¹ were obtained for 1,4 cyclohexanecarboxylic acid, (DCA). No adsorption for succinic acid, (SA), was observed on either the PAC or HAC, with only very limited adsorption observed on the CAC. This is not overly surprising, given the high solubilities of DCA and in particular SA, which likely limits the affinity these molecules have for the relatively hydrophobic surfaces of the solid adsorbents evaluated. This is, however, an interesting finding as this clearly implies that adsorption of naphthenic acid species that are similar to SA and DCA will likely be difficult with adsorbents that are not specifically modified for the purpose.

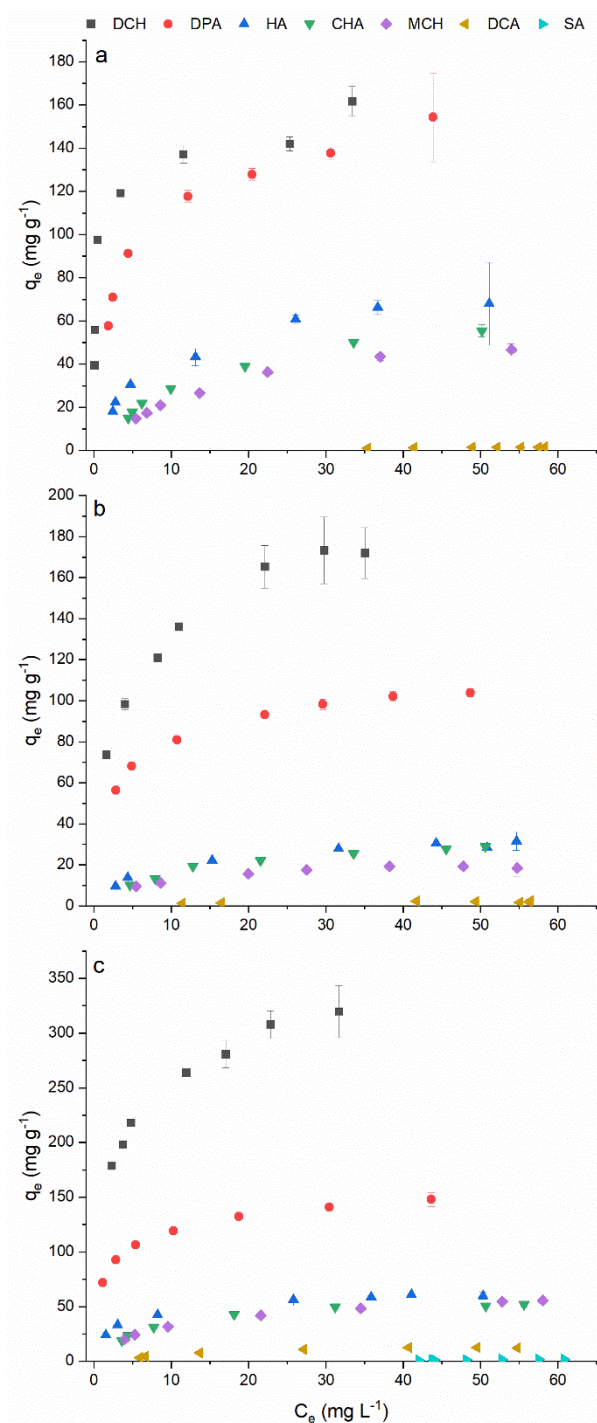


Figure 4.2: Adsorption isotherms for each model naphthenic acid on (a) PAC, (b) HAC, (c) CAC.

The adsorption performance also varies between the activated carbons explored. For several of the model naphthenic acids, adsorption was competitive on both the CAC and PAC, while in most cases adsorption was relatively poorer on the HAC. This trend can be further visualized when considering Figure 4.3, which shows the experimentally determined maximum adsorption capacities taken from the isotherms in Figure 4.2 for each model naphthenic acid, normalized to each activated carbon's respective specific surface areas. Clearly the PAC performs considerably better for many of the model naphthenic acids in comparison to both the CAC and HAC when normalized to the specific surface area.

The results depicted in Figure 4.3 demonstrate that the total specific

surface area is not the driving force for adsorption onto the surface of these

activated carbons. Instead, the surface functionality and likely key physicochemical properties of the model naphthenic acids are driving adsorption.

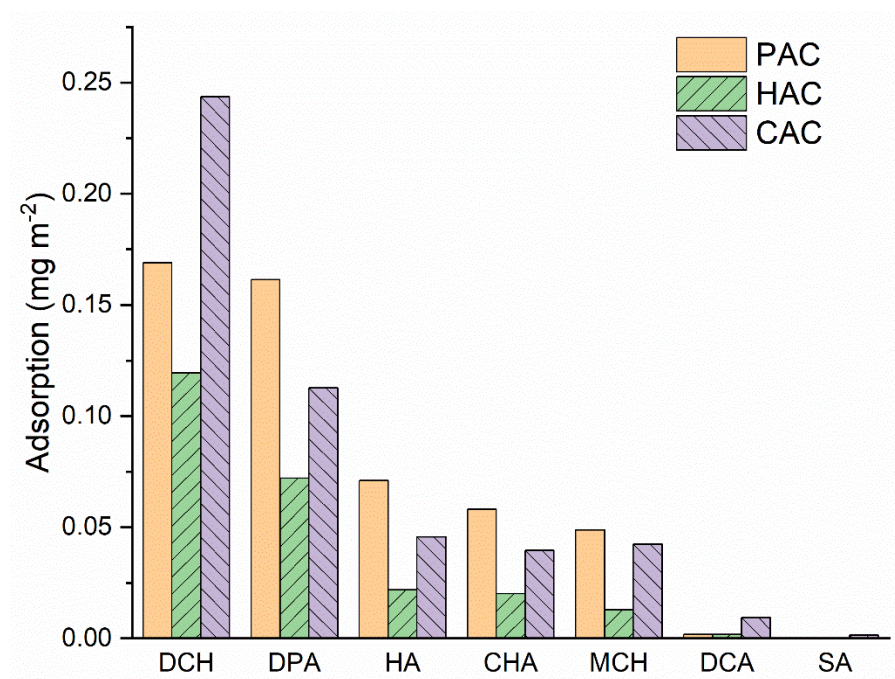


Figure 4.3: Maximum experimentally determined adsorption capacities of each model naphthenic acid normalized to total specific surface area of each activated carbon.

4.4.1 Model Evaluation of Adsorption Isotherms

The evaluation of adsorption isotherm modelling can be seen in Table 4.3, in which the reduced χ^2 , adjusted R^2 and AIC_c values for the best representative model for each adsorption system are displayed. ΔI values from EQ11 of less than 2 are generally considered acceptable, meaning that, in our case, both isotherm models adequately represent the adsorption isotherm (Eder et al., 2021). This was the case in several instances, so to differentiate the best representing isotherm model, the reduced χ^2 and adjusted R^2 were compared as well. The fitted parameters for the best representative models for each

adsorption system are displayed in **Error! Reference source not found..**

Despite the Freundlich model often being used to represent adsorption onto activated carbon in the literature(Tran et al., 2017), the Langmuir model was consistently more appropriate to represent several of the model naphthenic acid adsorption systems here. This is likely due to the Freundlich model's inability to represent the proportionality between sufficiently low C_e and q_e values, or the predicted saturation behavior observed at high C_e values when a complete isotherm is achieved(Ayawei et al., 2017). Most of the adsorption isotherms for heptanoic acid, (HA), cyclohexane acetic acid, (CHA), and 2-methyl-1-cyclohexanecarboxylic acid, (MCH), were represented best by the Langmuir model as indicated by the low reduced χ^2 and high adjusted R^2 values shown in Table 4.3. This implies that the activated carbon surfaces contain energetically equivalent adsorption sites with a homogeneous surface, as this is one of the main assumptions of the Langmuir model.

Activated carbon is not generally considered to have a uniform surface. However, there are cases in which the Langmuir model has suitably represented adsorption systems containing activated carbon, when this assumption of a homogenous surface is not fulfilled(Worch, 2012). For physisorption the range of energies associated with adsorption sites based on hydrophobic and/or hydrogen bonding is relatively small in comparison to higher energy interactions, such as specific chemical bond formation between an adsorbate and adsorbent(Tran et al., 2016). This may be adequate to allow the surface to be described as

homogeneous, with respect to small energy differences between physisorption sites.

Even for the MCH and HA isotherms on the CAC represented best by the Redlich-Peterson and Sips model respectively, the heterogeneity factor in both models, is relatively close to unity (as shown in Table 4.3), implying more energetically uniform adsorption sites on the activated carbon. DPA, although not modelled well by the Langmuir expression, also contained heterogeneity factors for the Redlich-Peterson and Sips modeling that were still relatively close to unity. DCH isotherms were best represented by either the Redlich-Peterson or Sips expressions. Interestingly though, the heterogeneity factors obtained from Sips modelling of DCH onto the CAC and HAC produced much lower values implying that a more variable energy distribution at the adsorption sites for this compound may exist on these two activated carbons. Although, DCA was modeled well by the Langmuir expression for adsorption onto the CAC, all isotherm models used to represent the DCA isotherms on the PAC and HAC, were poorly fit. This can be observed in Table 4.3 in which low R^2 values were obtained even for the best fitted isotherm model for DCA onto PAC and HAC. This was likely due to the low adsorption achieved on the PAC and HAC resulting in only a partial isotherm(Tran et al., 2017).

Table 4.3: Model evaluation for adsorption isotherms of model naphthenic acids.

Model NA	Adsorbent	Best Model	X ²	Adj R ²	AIC _c
DCH	PAC	RP	74.22	0.9645	40.23
	HAC	Sips	17.64	0.9883	30.17
	CAC	Sips	20.36	0.9933	31.18
DPA	PAC	RP	15.97	0.9876	29.48
	HAC	Sips	0.6168	0.9982	6.700
	CAC	RP	0.2683	0.9996	0.8738
HA	PAC	Langmuir	7.962	0.9821	19.17
	HAC	Langmuir	1.501	0.9799	7.489
	CAC	Sips	0.9872	0.9954	9.993
CHA	PAC	Langmuir	1.022	0.9960	4.794
	HAC	Langmuir	0.5111	0.9904	-0.0539
	CAC	Langmuir	1.183	0.9936	5.824
MCH	PAC	Langmuir	0.6351	0.9962	1.467
	HAC	Langmuir	0.4848	0.9692	-0.4234
	CAC	RP	0.1800	0.9991	-1.921
DCA	PAC	Langmuir	0.00528	0.8912	-32.05
	HAC	Langmuir	0.1165	0.4756	-10.40
	CAC	Langmuir	0.419	0.9736	-1.444

Table 4.4: Fitted parameters from isotherm modelling of the best representative models for each adsorption system.

Model NA	Adsorbent	Best Model	Langmuir		Sips			Redlich Peterson		
			Q_0 (mg/g)	K_L (L/mg)	Q_{ms} (mg/g)	K_s (L/mg) ^{β_s}	$β_s$	K_R (L/g)	a_R (L/mg) ^g	g
DCH	PAC	RP						887.7	7.489	0.9275
	HAC	Sips			284.8	0.2624	0.5147			
	CAC	Sips			670.1	0.2682	0.3575			
DPA	PAC	RP						80.51	0.846	0.8673
	HAC	Sips			129.9	0.4191	0.5869			
	CAC	RP						244.6	2.605	0.876
HA	PAC	Langmuir	78.96	0.1205						
	HAC	Langmuir	34.26	0.1371						
	CAC	Sips			74.51	0.3746	0.628			
CHA	PAC	Langmuir	72.71	0.0639						
	HAC	Langmuir	35.06	0.0841						
	CAC	Langmuir	58.37	0.1485						
MCH	PAC	Langmuir	62.87	0.0571						
	HAC	Langmuir	22.05	0.1304						
	CAC	RP						11.21	0.3743	0.8259
DCA	PAC	Langmuir	7.736	0.0045						
	HAC	Langmuir	2.553	0.0877						
	CAC	Langmuir	17.67	0.0519						

4.5 Influence of Naphthenic Acid Physiochemical Properties on Adsorption Capacity

Although the uptake capacity of model naphthenic acids varied from one adsorbent to another in Figure 4.2, what is more interesting is how certain model naphthenic acids consistently adsorb poorly relative to other naphthenic acid species, regardless of the activated carbon explored. This consistency in uptake affinity observed from one model naphthenic acid to the next was further explored through a series of linear correlation tests with respect to key physicochemical properties. Hydrophobicity for instance, has been seen as an important variable for adsorption of nonpolar organic contaminants onto activated

carbon (Sophia A. and Lima, 2018) and has often been represented in the literature through the octanol water partition coefficient. When dealing with ionizable species such as naphthenic acids however, the pH dependant

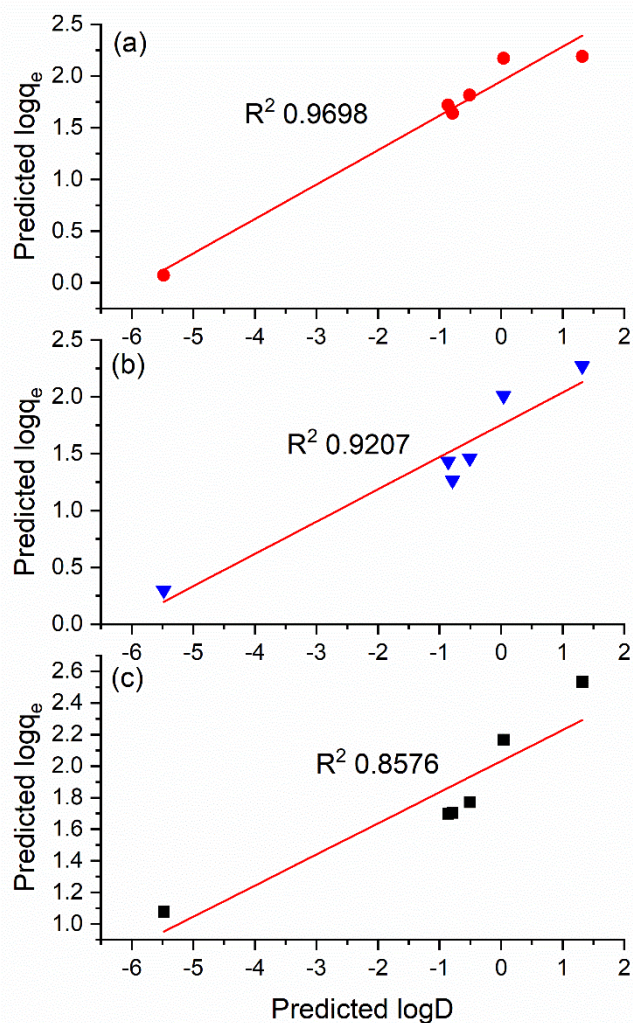


Figure 4.4: Relationships between the predicted distribution coefficients ($\log D$) and predicted $\log q_e$, based on isotherm modelling for a fixed C_e of 40 mg L^{-1} on (a) PAC, (b) HAC, and (c) CAC.

distribution coefficient ($\log D$) is considered more suitable to represent the hydrophobicity of organic species. Figure 4.4:

Relationships between the predicted distribution coefficients ($\log D$) and predicted $\log q_e$, based on isotherm modelling for a fixed C_e of 40 mg L^{-1} on (a) PAC, (b) HAC, and (c) CAC. displays linear correlation tests conducted on predicted naphthenic acid $\log D$ values versus the logarithm of adsorption capacities obtained through isotherm

modelling at a fixed C_e of 40 mg L^{-1} , as similarly described in Ridder et

al (de Ridder et al., 2010). The high R^2 values indicate that the predicted $\log D$ values are strongly correlated to adsorption performance of the model naphthenic acids regardless of the activated carbon evaluated. This implies hydrophobic interactions between the model naphthenic acids and the adsorbent

surface, akin to physisorption, may be occurring. It is of course worth acknowledging the limited sample size employed for these linear correlations. However, these results are consistent with previous works that have identified the importance of solute hydrophobicity with considerably more organic contaminants evaluated for their adsorption onto activated carbon (de Ridder et al., 2010).

Other interactions with the activated carbon surface should also be considered. All naphthenic acids contain at least one electron acceptor, through the carboxylate functional group, under the alkaline conditions tested. Certain oxygen functionality present on the surface of activated carbon, should allow for stronger electrostatic interactions to exist between the model naphthenic acids and the surface. These interactions should be influenced by the PZC of each adsorbent. PAC and HAC bear a PZC of 6.5 and 4 respectively, meaning that acidic oxygen functional groups are likely negatively charged under the pH of 8 evaluated in the adsorption tests. This would limit the number of adsorption sites available on these adsorbents, while hydrogen bonding with hydroxyl functionality on the surface would still be possible on PAC and HAC. Additionally, hydrogen bonding may partially explain, for instance, why the HAC adsorbs most model naphthenic acids considerably less effectively than the PAC and CAC. The atomic percent of oxygen on the HAC surface is considerably less than that on the PAC and CAC, which may imply less hydrogen bonding opportunities between surface hydroxyl functionality and model NAs, reducing overall adsorption affinity. Additionally, the presence of highly electronegative

phosphates and pyrophosphates, found uniquely on the HAC surface, could impose strong electrostatic repulsion interactions with model naphthenic acid adsorbates, further limiting adsorption affinity. This is further supported by comparison of the HAC with and without the heat treatment process described in Chapter 2, section 2.2.2. This heat treatment produced a reduction in phosphate content on the HAC surface and saw improved model naphthenic acid uptake.

4.6 Conclusion

The highly variable adsorption affinity of model naphthenic acid species displayed above should help researchers better identify which species are likely to be recalcitrant towards adsorption onto activated carbons. These results should also be applicable to any porous adsorbents that share similar surface functionality with the activated carbons used in this thesis. This becomes more obvious when considering the importance of key physiochemical properties of the model naphthenic acids towards uptake. Hydrophobicity was identified to be important for adsorption affinity onto activated carbon. This study strongly points to physisorption as the main mechanism of adsorption of naphthenic acid species. Although having an activated carbon with a hydrophobic surface is beneficial for hydrophobic interactions between model species, hydrogen bonding with surface site oxygenated species is likely important as well. Reduced adsorption capacities observed for the HAC for nearly all model species relative to the other two adsorbent carbons evaluated suggests the presence of certain oxygenated species are favorable for increasing adsorption affinity. We see evidence of this when considering the reduced atomic percent oxygen on the

HAC surface relative to the PAC and CAC. Modifying surface functionality to increase these favorable interactions with recalcitrant NA species should be a future direction that is taken to maximize the adsorption capabilities of activated carbons.

5 Adsorption Thermodynamics of Model Naphthenic Acids

5.1 Introduction

The uptake of naphthenic acids onto activated carbon has previously been shown to likely occur through relatively weak hydrophobic interactions with the surface, or through hydrogen bonding. These proposed mechanisms are largely based on the chemical structures of the model naphthenic acids investigated and on a clear understanding of the surface functionality of the activated carbon. Confirming these mechanisms is a critical step towards finding ways to enhance the uptake of recalcitrant naphthenic acids. This is possible through an evaluation of adsorption thermodynamics. Standard state thermodynamic values and isosteric enthalpy of adsorption are useful parameters for validating uptake mechanisms for aqueous contaminants. Within this chapter, uptake kinetics at different temperatures were used to explore activation energy of adsorption using kinetic modelling. This was then followed by an evaluation of adsorption equilibrium behavior, under a range of temperatures to determine the standard state thermodynamic values of ΔG° , ΔH° , ΔS° and isosteric heats of adsorption, $\Delta_{ist}H$, for several model naphthenic acid species adsorbed onto a petroleum coke activated carbon, PAC. Although some work has involved model naphthenic acid adsorption onto activated carbon (Iranmanesh et al., 2014; Martinez-Iglesias et al., 2015; Niasar et al., 2016; Sarkar, 2013; Strong et al., 2023b), a thermodynamic analysis involving standard state parameters and isosteric heats of adsorption, to my knowledge have not been performed with activated carbon or any similar adsorbents.

As highlighted by Tran et al, standard state thermodynamic parameters of adsorption systems have been calculated through a variety of different approaches (Tran et al., 2017). In this work, a common approach that involves adsorption isotherm modelling of equilibrium data over a small temperature range using two different modelling approaches was used (Piccin et al., 2017). Both the Langmuir and Sips models were used to represent the adsorption isotherms of model naphthenic acids. Fitting constants from the isotherm modelling were used to approximate the equilibrium constant taking into consideration a reference state and the activity of the model naphthenic acids, which allows use of the van't Hoff expression to determine standard state parameters (Ghosal and Gupta, 2017). The magnitude of the ΔH° was used to discern between physisorption versus chemisorption (Lima et al., 2021; Liu, 2009), and then compared with the previously proposed uptake mechanisms presented in chapter 4. Isosteric heat of adsorption calculations, based on isotherm modelling, were used to evaluate PAC surface homogeneity, which is useful in checking the logic of the methods used to determine the standard state thermodynamic parameters and give some further insights into adsorption behavior (Inglezakis and Zorpas, 2012; Salvestrini et al., 2014).

5.2 Materials & Methods

Within this chapter, three model naphthenic acids were explored, namely heptanoic acid, cyclohexylacetic acid, and benzoic acid. Benzoic acid, like heptanoic acid and cyclohexylacetic acid, was included within this work due to its

low affinity for the surface of PAC. Adsorption isotherms and all subsequent modelling analysis followed the procedures outlined within chapter 2.

5.3 Activation Energy of Adsorption

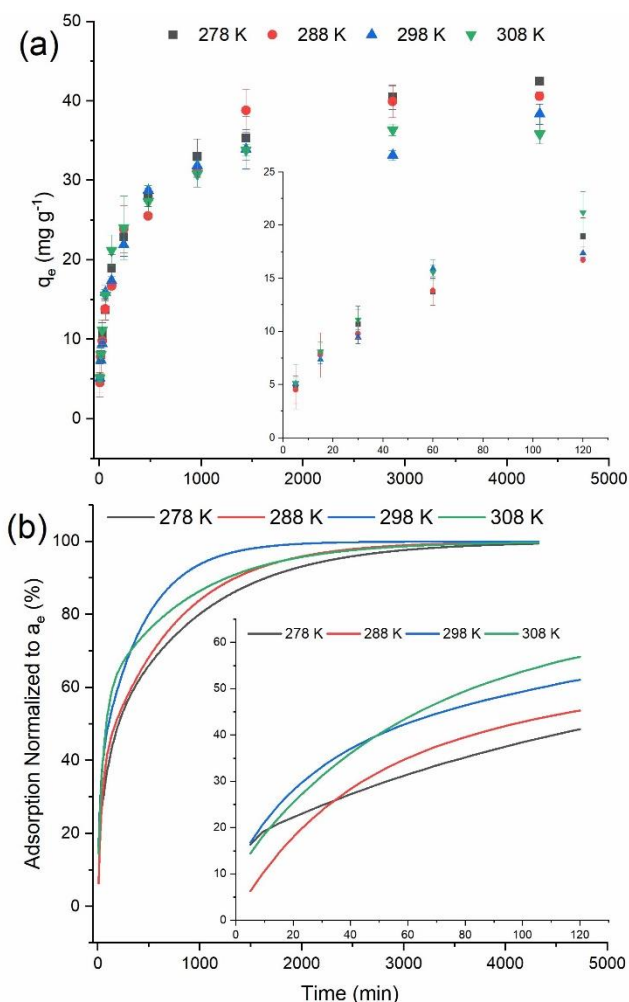


Figure 5.1: (a) Adsorption kinetics of CHA onto PAC at four different controlled temperatures. (b) kinetic modelling for CHA adsorption kinetics normalized to the predicted equilibrium capacity, a_e .

The adsorption kinetics for 3 model naphthenic acids, heptanoic acid (HA), cyclohexylacetic acid (CHA), and benzoic acid (BA) onto PAC, was determined within the temperature range of 278 to 308 K.

An example of these kinetics is shown in Figure 5.1 for CHA.

Determination of activation energy from the uptake kinetics shown in Figure 5.1 requires there to be a change in the kinetic uptake as a function of temperature. Although slight differences in the kinetics are apparent from Figure 5.1 (a),

overlap of the kinetic plots along

with slight differences in equilibrium behavior in the later time points from one temperature to another largely obscures visual differences in adsorption rates.

Kinetic modelling using the m-exp model, EQ5 from Chapter 2 section 2.4, helps address this issue. This is made visually clearer in Figure 5.1 (b), which shows

the predicted m-exp model fit for the CHA kinetics normalized to the predicted max adsorption capacity (a_e) from m-exp modelling. As seen in

Table 5.1, the predicted a_e values are slightly different for the kinetics produced at different temperatures, so by simply normalizing each predicted m-exp kinetics curve to its respective a_e value, a clearer depiction of differences in uptake rates can be observed in the bottom graph of Figure 5.1.

Table 5.1: m-exp model fitting assessed by both the R^2 and reduced X^2 for model naphthenic acid adsorption. The time to reach 50% ($t_{1/2}$) and 75% ($t_{3/4}$) uptake, based on m-exp modelling, are shown. The m-exp model parameter showing the predicted equilibrium capacity (a_e) is also displayed.

CHA					
T (K)	R^2	Reduced X^2	$t_{1/2}$ (min)	$t_{3/4}$ (min)	a_e (mg g ⁻¹)
278	0.994	2.790	204	782	42.01
288	0.986	6.220	169	670	40.09
298	0.981	6.602	104	402	35.43
308	0.999	0.327	83	471	36.43
HA					
T (K)	R^2	Reduced X^2	$t_{1/2}$ (min)	$t_{3/4}$ (min)	a_e (mg g ⁻¹)
278	0.991	7.600	328	1560	59.52
288	0.990	6.389	109	635	50.74
298	0.975	14.55	83	648	50.24
308	0.966	17.57	70	292	45.86
BA					
T (K)	R^2	Reduced X^2	$t_{1/2}$ (min)	$t_{3/4}$ (min)	a_e (mg g ⁻¹)
278	0.992	1.991	35	225	46.33
288	0.997	0.563	13	182	42.39
298	0.961	16.55	34	255	44.15
308	0.997	0.379	10	95	37.30

Adsorption half times that were calculated from m-exp modelling, shown in Table 5.1, indicate that the adsorption rates for all three model naphthenic acids do generally increase as temperature rises. There are some exceptions to this. For instance, the 298 K benzoic acid uptake kinetics clearly is an outlier as the

adsorption half time is closer to that obtained for the benzoic acid 278 K uptake kinetics. This is made clearer when considering the time to reach 75% adsorption ($t_{3/4}$), which is also shown in

Table 5.1.

Arrhenius plots were produced for each model naphthenic acid, using the same procedure as Marczewski et al, in which the natural logarithm of adsorption half time, was plotted against the inverse of temperature (Marczewski et al., 2016). Certain adsorption half time values displayed in

Table 5.1 were omitted from their respective Arrhenius plots to improve linearity, such as that from the 298 K benzoic acid kinetics. However, each Arrhenius plot still maintained a minimum of three data points. High linearity as demonstrated by the high R^2 values shown in Table 5.2, was achieved for both HA and CHA, while poor linearity was observed for the benzoic acid Arrhenius plot. The activation energies approximated from these Arrhenius plots were all within the same order of magnitude for each model naphthenic acid, ranging approximately from 14 to 40 kJ mol^{-1} .

Table 5.2: Calculated activation energies of adsorption (E_a) for each model naphthenic acid using two different approaches. R^2 values are included to assess linearity for the Arrhenius plot used.

	Using $t_{1/2}$		Using $t_{3/4}$	
	E_a (kJ mol^{-1})	R^2	E_a (kJ mol^{-1})	R^2
HA	16.36 ± 1.86	0.987	38.19 ± 7.22	0.966
CHA	22.64 ± 2.95	0.967	12.15 ± 0.70	0.997
BA	27.32 ± 14.50	0.780	20.88 ± 2.54	0.985

A potential concern with the approach described by Marczewski and al to approximate activation energy, may be the arbitrary nature of choosing half times of adsorption instead of adsorption rate constants (Marczewski et al., 2016). The times to reach 75 % adsorption ($t_{3/4}$) were also used to approximate activation energies in replace of $t_{1/2}$ values. Similarly, clear outliers were omitted to improve linearity while at least three $t_{3/4}$ values were used for each Arrhenius plot. The activation energies in Table 5.2, based on using $t_{3/4}$ values, differ slightly from the activation energies obtained from adsorption half times. The largest difference was observed with heptanoic acid in which the approach using $t_{3/4}$ values produced an activation energy of 38 kJ mol⁻¹ in comparison to 16 kJ mol⁻¹. These differences obtained from the two separate approaches, although significant, still fall within empirical ranges for activation energies expected for physisorption (Inglezakis and Zorpas, 2012). These values agree with relatively weak Vander waal interactions and possible hydrogen bonding mechanisms of adsorption that were postulated in Chapter 4 for model naphthenic acids onto PAC.

5.4 Standard State Thermodynamic Adsorption Parameters

5.4.1 Langmuir Approach

Adsorption isotherms for the model naphthenic acids HA, CHA, and BA at temperatures ranging from 278 to 308 K are shown in Fig. 19. Isotherm modelling using the Langmuir model, EQ6 from chapter 2, section 2.5.1, is also included in Figure 5.2: Adsorption isotherms on PAC for a; Heptanoic acid. b; Cyclohexylacetic acid. c; Benzoic acid. Langmuir modelling is superimposed on each respective isotherm.

. The fitting analyses for the Langmuir expression are presented in Table 5.3, which indicate an acceptable model fit for each model naphthenic acid adsorption isotherm. The Langmuir fitted parameters are also

included in Table 5.3 and show a general increase in the Langmuir constant, K_L , as temperature decreases for each model naphthenic acid. This is to be expected given the slight change in curvature observed for the isotherms presented in Figure 5.2: Adsorption isotherms on PAC for a; Heptanoic acid. b; Cyclohexylacetic acid. c; Benzoic acid. Langmuir modelling is superimposed on each respective isotherm.

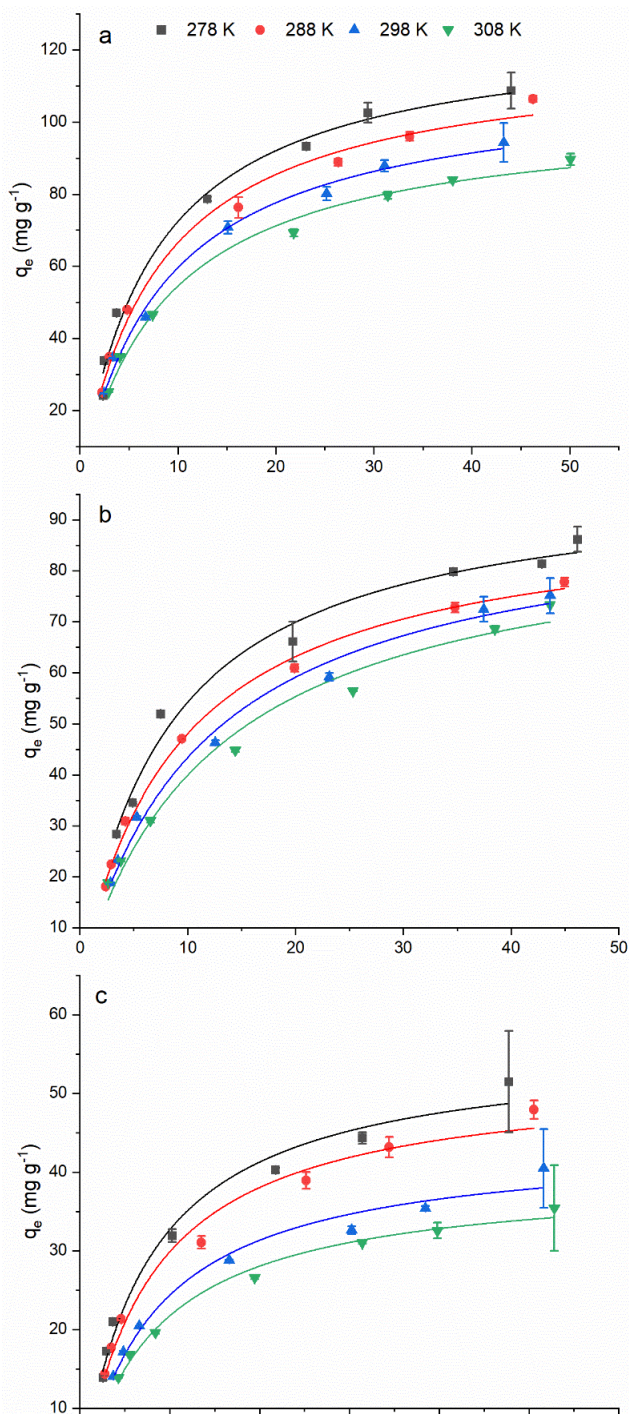


Figure 5.2: Adsorption isotherms on PAC for a; Heptanoic acid. b; Cyclohexylacetic acid. c; Benzoic acid. Langmuir modelling is superimposed on each respective isotherm.

as temperature decreases.

Following the method proposed by several authors, the Langmuir constant was used to approximate the equilibrium constant, K_c , presented in EQ12 and EQ13, chapter 2, section 2.7.1 (Ghosal and Gupta, 2017; Liu, 2009). An example of the van't Hoff plot based on the use of EQ12 is shown in Figure 5.3. Acceptable linearity for each van't Hoff plot (>0.9) was achieved using the Langmuir approach to approximate K_c (Tran et al., 2017). Standard state thermodynamic parameters using the Langmuir model approach can be seen in Table 5.4. ΔG° similarly varies with temperature from -27 to -30 kJ mol⁻¹ for each model naphthenic acid.

Both HA and BA yield very similar ΔH° and ΔS° values, while some difference was

observed for CHA, having a slightly lower ΔH° and ΔS° . These differences, however, do not change the interpretation from these values. ΔH° with absolute values below 200 kJ mol^{-1} are consistent with physisorption (Lima et al., 2021). All three model naphthenic acids exhibit relatively small ΔH° , suggesting similar low energy interactions occurring for each model naphthenic acid with the PAC surface.

Table 5.3: Fitting analysis and parameters obtained from Langmuir modelling of isotherms produced for each model naphthenic acid.

	Langmuir Parameters			Fitting Analysis	
	T (K)	$Q_0 \text{ (mg g}^{-1}\text{)}$	$K_L \text{ (L mg}^{-1}\text{)}$	R^2	reduced χ^2
HA	278	126.3 ± 4.94	0.1344 ± 0.0170	0.988	16.42
	288	119.5 ± 4.11	0.1255 ± 0.0143	0.990	11.78
	298	111.2 ± 3.26	0.1155 ± 0.0105	0.994	5.855
	308	102.9 ± 2.77	0.1125 ± 0.0102	0.993	5.433
CHA	278	98.34 ± 3.46	0.1231 ± 0.0148	0.985	9.909
	288	92.17 ± 2.03	0.1089 ± 0.0070	0.997	2.263
	298	92.95 ± 3.54	0.0875 ± 0.0093	0.992	5.097
	308	90.22 ± 5.55	0.0793 ± 0.0134	0.981	10.77
BA	278	56.01 ± 2.29	0.1402 ± 0.0182	0.984	4.011
	288	52.39 ± 2.04	0.1327 ± 0.0169	0.984	3.303
	298	43.94 ± 1.91	0.1245 ± 0.0179	0.976	2.956
	308	39.55 ± 1.03	0.1222 ± 0.0107	0.990	0.845

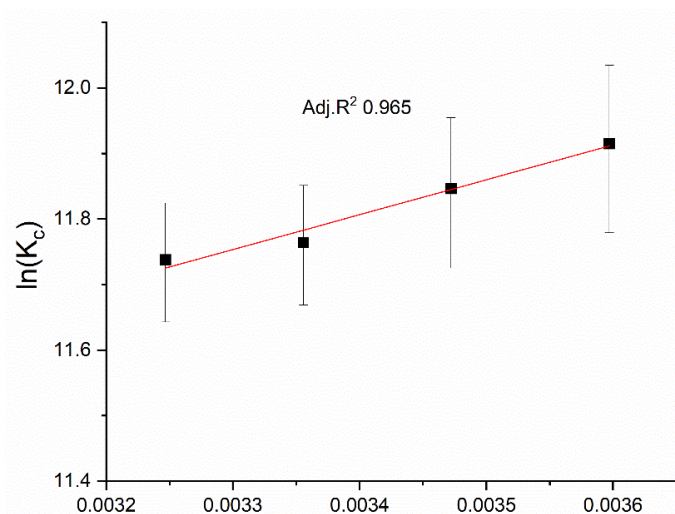


Figure 5.3: van't Hoff plot produced using the Langmuir approach for HA.

Some have criticized the use of the Langmuir model to approximate standard state parameters, even if the activity of the adsorbing species and proper reference state is considered in accordance with EQ13 (Vanore et al., 2017). This is largely due to the

underlying assumptions of the Langmuir model which often are not fulfilled within aqueous adsorption systems. This extends to several assumptions. As described by Salvestrini et al, the Langmuir model assumes a finite number of available adsorption sites, implying that the maximum predicted adsorption capacity should not change with changing temperature and will only form a monolayer (Salvestrini et al., 2014). We see clear evidence that the Q_o parameter within Table 5.3 does increase with decreasing temperature for each model naphthenic acid, which may be due to multilayer adsorption more favorably occurring at lower temperatures. This raises some caution in how to interpret the standard state parameters developed by the Langmuir approach.

Table 5.4: Standard state thermodynamic parameters for the adsorption of model naphthenic acids onto PAC using the Langmuir approach.

HA	T (K)	ΔG° (kJ mol ⁻¹)	ΔH° (kJ mol ⁻¹)	ΔS° (J mol ⁻¹ K ⁻¹)
	278	-27.53 ± 0.021	-4.425 ± 0.483	83.12 ± 1.66
	288	-28.36 ± 0.005		
	298	-29.19 ± 0.012		
	308	-30.02 ± 0.028		
CHA				
	278	-27.55 ± 0.050	-10.74 ± 0.910	60.47 ± 3.09
	288	-28.15 ± 0.019		
	298	-28.76 ± 0.012		
	308	-29.36 ± 0.043		
BA				
	278	-27.48 ± 0.020	-3.494 ± 0.442	86.28 ± 1.52
	288	-28.34 ± 0.005		
	298	-29.21 ± 0.010		
	308	-30.07 ± 0.025		

5.4.2 Sips Approach

Given the uncertainty in the interpretation of the standard state parameters obtained through Langmuir modelling, a second approach using the Sips isotherm model, EQ9 chapter 2, section 2.5.4, was used to approximate the

standard state thermodynamic adsorption parameters of each model naphthenic acid. The obtained parameters and analysis for the Sips model fitted to each respective adsorption isotherm is seen in Table 5.5. The Sips constant K_s , was used to approximate the equilibrium constant according to EQ14, chapter 2, section 2.7.1.

Table 5.5: Model parameters and fitting analysis for the Sips model fitted to each of the model naphthenic acid isotherms.

	T (K)	Sips Parameters			Fitting Analysis	
		Q_{ms} (mg g ⁻¹)	K_s (L mg ⁻¹) ^{BS}	β_s	R^2	reduced χ^2
HA	278	128.4 ± 16.97	0.136 ± 0.022	0.974 ± 0.195	0.988	20.44
	288	148.4 ± 26.47	0.128 ± 0.016	0.764 ± 0.128	0.994	8.715
	298	127.0 ± 15.28	0.123 ± 0.011	0.837 ± 0.110	0.996	4.818
	308	127.4 ± 16.97	0.122 ± 0.010	0.756 ± 0.098	0.997	2.917
CHA	278	100.8 ± 15.23	0.128 ± 0.032	0.954 ± 0.261	0.985	12.32
	288	96.7 ± 7.373	0.113 ± 0.009	0.933 ± 0.093	0.997	2.523
	298	128.1 ± 24.19	0.088 ± 0.011	0.738 ± 0.092	0.997	2.222
	308	398.7 ± 272.7	0.031 ± 0.020	0.524 ± 0.048	0.999	0.561
BA	278	74.94 ± 17.38	0.141 ± 0.023	0.695 ± 0.139	0.992	2.574
	288	81.28 ± 18.65	0.126 ± 0.022	0.619 ± 0.096	0.996	1.014
	298	78.09 ± 49.64	0.117 ± 0.059	0.552 ± 0.195	0.987	1.912
	308	53.84 ± 6.971	0.143 ± 0.010	0.652 ± 0.078	0.998	0.200

Despite excellent fitting for the Sips model to each adsorption isotherm, conversion of K_s to K_c , produced obvious outliers for the van't Hoff plots for each

model naphthenic acid. Removal of these outliers, while still maintaining a minimum of three data points, improved linearity in each van't Hoff plot significantly. However, the R^2 obtained for the CHA van't Hoff plot was just over the 0.9 recommended threshold for linearity. This resulted in a higher degree of uncertainty in the standard state parameters obtained for CHA when using the Sips model, which is observed in the high error of ΔH° and ΔS° values in Table 5.6. Significant differences were observed for ΔH° obtained through Sips modelling in comparison to the respective values obtained through Langmuir modelling. For all three model naphthenic acids, ΔH° significantly decreased with the Sips approach, perhaps reflecting the fact that the Sips model is not restricted to the same assumptions as the Langmuir model. The Sips model assumes adsorbate interactions occur and that different adsorption sites are possible. This may indicate the Sips model to be a better choice to represent the adsorption of naphthenic acids onto PAC. Despite the differences in standard state parameters obtained with respect to the Langmuir approach, the ΔH° values are still well within the empirical range associated with physisorption. Although ΔG° values saw minimal change with the Sips approach, ΔS° values for all three model species did change significantly. For both CHA and BA, ΔS° changed in sign from positive to negative. However, the error in the CHA ΔS° was on the same order of magnitude as the ΔS° value and is likely a reflection of the poorer van't Hoff plot produced.

Table 5.6: Standard state thermodynamic parameters for model naphthenic using the Sips modelling approach.

HA	T (K)	ΔG° (kJ mol ⁻¹)	ΔH° (kJ mol ⁻¹)	ΔS° (J mol ⁻¹ K ⁻¹)
----	-------	--	--	---

CHA	278	-27.46 ± 0.0609	-17.02 ± 37.54	37.54 ± 4.074
	288	-27.83 ± 0.0201		
	298	-28.21 ± 0.0206		
	308	-28.58 ± 0.0613		
BA	278	-27.55 ± 0.3750	-38.29 ± 12.52	-38.61 ± 43.67
	288	-27.17 ± 0.0618		
	298	-26.78 ± 0.4985		
	308	-26.40 ± 0.9352		
	278	-25.54 ± 0.0447	-37.03 ± 1.017	-41.32 ± 3.496
	288	-25.12 ± 0.0098		
	298	-24.71 ± 0.0252		
	308	-24.30 ± 0.0602		

5.4.3 Isosteric Heat of Adsorption

The isosteric heat of adsorption, $\Delta_{ist}H$, was used to evaluate surface site homogeneity of PAC. To do this, the Langmuir model parameters established in Table 5.3, alongside the rearranged form of the Langmuir model, EQ16, chapter 2, section 2.7.2, were used to first determine C_e values as a function of q_e . By plotting the natural logarithm of C_e versus the inverse of temperature at several fixed q_e values, the $\Delta_{ist}H$ as a function of surface coverage could be assessed. An example of these $\ln C_e$ versus $1/T$ plots for heptanoic acid, are displayed in Figure 5.4: Plots of $\ln C_e$ versus $1/T$ for fixed adsorption capacities, q_e , for heptanoic acid. For each fixed q_e linear regressions are displayed.. The $\Delta_{ist}H$ values for each fixed q_e were then evaluated by use of the slope of a linear regression.

The resulting $\Delta_{ist}H$ for each model naphthenic acid as a function of surface coverage is shown in Figure 5.5: $\Delta_{ist}H$ versus q_e for each model naphthenic acid

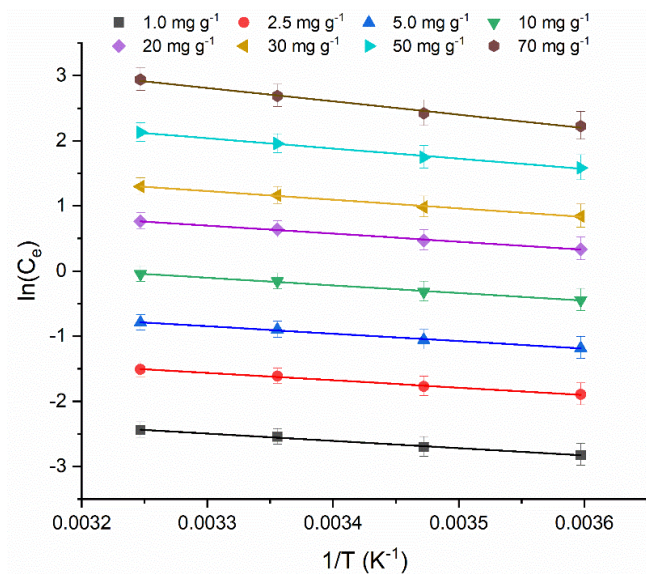


Figure 5.4: Plots of $\ln C_e$ versus $1/T$ for fixed adsorption capacities, q_e , for heptanoic acid. For each fixed q_e linear regressions are displayed.

adsorption system.. Clearly $\Delta_{ist}H$ decreases with increasing q_e , or increasing surface coverage, which may imply either the PAC surface is not homogeneous and/or rising interactions between adjacently adsorbed model naphthenic acids (Inglezakis and Zorpas, 2012). It

has been postulated that there are different adsorption sites

present on the PAC surface for model naphthenic acids to interact with, which may partly explain the variable $\Delta_{ist}H$. Interestingly, the decrease in $\Delta_{ist}H$ as surface coverage increases is more pronounced for benzoic acid than either HA or CHA. This may be explained by higher energy interactions between adjacently adsorbed benzoic acid molecules due to π π stacking, which would not occur for either HA or CHA. The variable $\Delta_{ist}H$ further emphasizes that assumptions underlying the Langmuir model are not upheld for these adsorption systems, as $\Delta_{ist}H$ should numerically equal the ΔH° produced through the Langmuir approach (Salvestrini et al., 2014). Each model naphthenic acid plot, of $\Delta_{ist}H$ versus q_e , was fitted using a simple exponential decreasing model which is also shown in Figure 5.5: $\Delta_{ist}H$ versus q_e for each model naphthenic acid adsorption

system.. The extrapolation of this model allowed for an approximation of the

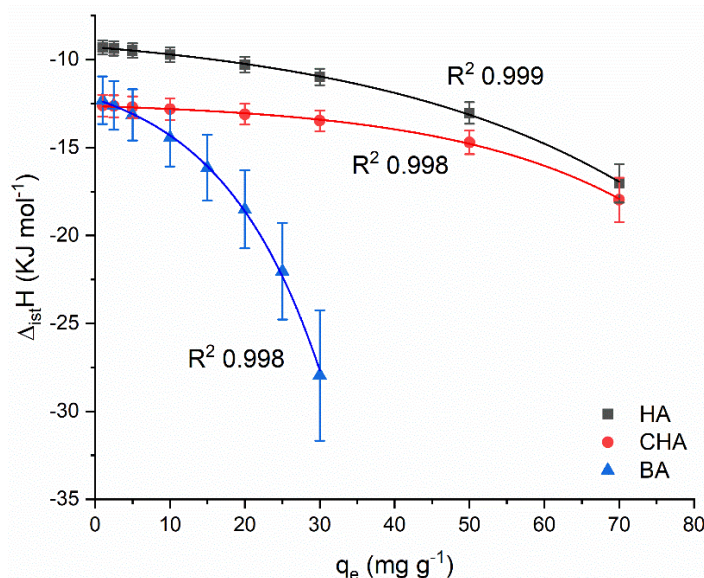


Figure 5.5: $\Delta_{\text{ist}}H$ versus q_e for each model naphthenic acid adsorption system.

isosteric heat of adsorption at zero coverage which was determined to be -8.0, -12.3, and -10.4 kJ mol⁻¹ for HA, CHA, and BA respectively.

The isosteric heat of adsorption values at zero coverage are much closer to the respective standard state enthalpy changes obtained

through Langmuir modelling, which may imply that the ΔH° values from Table 5.4 are only rough estimates at zero coverage and not from the entire equilibrium range.

5.5 Conclusion

The adsorption thermodynamics of several model naphthenic acids were presented. Activation energies were determined through a kinetic modelling approach using either $t_{1/2}$ or $t_{3/4}$ values. E_a values for both methods ranged from approximately 14 to 45 kJ mol⁻¹ for all three model naphthenic acids which all fall within expected ranges for physisorption. A detailed evaluation of two different modelling approaches of equilibrium behavior were used to approximate standard state parameters. Although some differences in standard state values did exist between the different modelling approaches used, more importantly the

ΔH° remained within the same range expected for physisorption to occur. This was further supported with the isosteric heat of adsorption determined for each model naphthenic acid. Although $\Delta_{ist}H$ was shown to vary as a function of surface coverage, the heat released during adsorption was still well within the expected range for physical adsorption mechanisms. These results further solidify that relatively weak hydrophobic interactions with the PAC surface, and/or hydrogen bonding with surface site hydroxyl functionality occur for model naphthenic acid uptake. This work strongly suggests that enhancements to certain surface functionality of activated carbon or any similar porous adsorbents should be the focus of future research towards tailoring the removal of recalcitrant naphthenic acids.

6 Conclusions

6.1 General Conclusions

In this work, the adsorption of a series of model naphthenic acid species were evaluated onto various activated carbons (AC) both in terms of uptake kinetics and equilibrium behavior. Physical properties most conducive to achieve fast

adsorption kinetics were identified. Modification of both the pore size distribution and adsorbent particle size can ensure adsorption equilibrium is achieved for naphthenic acids within a matter of hours, thus demonstrating the potential for optimizing adsorption kinetics using AC.

An important finding within this work was the variable adsorption capacities identified for structurally different model naphthenic acids onto activated carbon. These results clearly highlight the predicted persistence of certain naphthenic acids within OSPW that are treated with AC adsorbents, while also demonstrating that other naphthenic acids will more readily be removed through adsorption. The hydrophobicity of naphthenic acids was identified as an important physiochemical property for uptake onto activated carbon. Several mechanisms were proposed to explain the adsorption process of model naphthenic acids onto activated carbons based on the chemical structures of the individual species and a characterization of the surfaces of the adsorbent materials. Hydrophobic interactions between many model species and the activated carbon surface play a key role in the adsorption process. While hydrogen bonding between model species and surface site hydroxyl groups on activated carbon likely offer additional sites for adsorption to take place.

A thermodynamic analysis of the adsorption system containing model species and activated carbon was used to further support the proposed mechanisms of adsorption. The standard state enthalpy parameters calculated through both Langmuir and Sips modelling both imply that the dominate interactions happening between model species and the surface of AC are of low energy

interactions (physisorption). Isosteric heat of adsorption values demonstrated that the adsorption process is variable with surface coverage implying that rising adsorbate adsorbate interactions or multilayer adsorption may be occurring with rising surface coverage. Regardless, the range of isosteric heat of adsorption values determined for several model naphthenic acids are consistent with physisorption and help support the proposed mechanisms for adsorption of model naphthenic acids onto AC.

The work in this thesis should help future researchers identify recalcitrant naphthenic acids within OSPW and offer valuable insights into what modifications of activated carbon will need to be made to successfully target them. The insights gained through this work should extend to any porous adsorbent systems targeting naphthenic acids, thus providing a valuable resource on naphthenic acid adsorption behavior.

6.2 Future Work

1. Explore post treatment modification schemes for the surface of activated carbon that will tailor surface chemistry to allow uptake enhancements of recalcitrant model naphthenic acid species.
2. Explore the adsorption thermodynamics of more model naphthenic acids onto activated carbon to identify potential differences in adsorption behavior for structurally different species.

3. Investigate mass transfer kinetic models to more thoroughly characterize the uptake behavior of model naphthenic acids onto AC and to identify the rate limiting adsorption steps.

6.3 Contributions to Science

6.3.1 Publications

- After presenting at the Conference of Metallurgists 2022, abstracts were published within electronic proceedings.
 - Nazari, Elmira & Roy, Tyler & Strong, Oliver & Vreugdenhil, Andrew. (2023). Adsorption of Naphthenic Acids from Oil Sand Process-Affected Water (OSPW) Using Commercially Viable Petcoke-Sourced Activated Carbon. Proceedings of the 61st Conference of Metallurgists, COM 2022 pp 251–254
DOI: 10.1007/978-3-031-17425-4_35.
 - Tyler M Roy, Andrew J Vreugdenhil, Study of Adsorption Thermodynamics of Model Naphthenic Acids for Determining Adsorption Mechanism Using Commercially Viable Petroleum Coke-Activated Carbon, Proceedings of the 61st Conference of Metallurgists, COM 2022 pp 265-267
DOI: 10.1007/978-3-031-17425-4_38.

- In collaboration with Elmira Nazari and Oliver Strong I worked on a project that focused on naphthenic acid kinetics with petcoke derived activated carbons. The study is currently published in Heliyon.
 - Strong, O.K.L., Nazari, E., Roy, T., Scotland, K., Pede, P.R., Vreugdenhil, A.J., 2023. Transforming micropores to mesopores by heat cycling KOH activated petcoke for improved kinetics of adsorption of naphthenic acids. *Heliyon* 9.
<https://doi.org/10.1016/j.heliyon.2023.e13500>

- In collaboration with Elmira Nazari, I worked on a project that focused on evaluating the equilibrium behavior of a series of model naphthenic acids adsorbed to various activated carbon adsorbents. The study is currently published in the Journal of Environmental Sciences.
 - Roy, T. M., Nazari, E., Strong, O. K. L., Pede, P. R., & Vreugdenhil, A. J. (2025). The effect of adsorbent textural and functional properties on model naphthenic acid adsorption. *Journal of Environmental Sciences (China)*, 148, 27–37.
<https://doi.org/10.1016/j.jes.2024.01.003>

6.3.2 Conferences

- IUPAC CCCE, 2021, Canadian Chemistry Conference & Exhibition, virtual conference

I presented on the “*Characterization of Model Naphthenic Acid Adsorption on various Activated Carbon Adsorbents*”

- COM 2022, Conference of Metallurgy & Materials, Montreal, Quebec

I presented on the “*Adsorption Thermodynamics of Model Naphthenic Acids for Determining Uptake Mechanisms on Commercially Viable Petroleum Coke Sourced Activated Carbon*”

- IIES 2022, International Institute for Environmental Studies, Vietnam

I presented on “*Model Naphthenic acid adsorption isotherms with thermodynamic property Estimations onto Activated Carbon*”

- CSC 2023, Canadian Chemistry Conference and Exhibition, Vancouver

I presented on, “*Adsorption Thermodynamics of model Naphthenic Acids onto Activated Carbon*”

References

- Allen, E.W., 2008. Process water treatment in Canada's oil sands industry: II. A review of emerging technologies. *Journal of Environmental Engineering and Science*. <https://doi.org/10.1139/S08-020>
- Ayawei, N., Ebelegi, A.N., Wankasi, D., 2017. Modelling and Interpretation of Adsorption Isotherms. *J Chem*. <https://doi.org/10.1155/2017/3039817>
- Azad, F.S., Abedi, J., Iranmanesh, S., 2013. Removal of naphthenic acids using adsorption process and the effect of the addition of salt. *J Environ Sci Health A Tox Hazard Subst Environ Eng* 48, 1649–1654. <https://doi.org/10.1080/10934529.2013.815457>

- Bagheri, N., Abedi, J., 2009. Preparation of high surface area activated carbon from corn by chemical activation using potassium hydroxide. *Chemical Engineering Research and Design* 87, 1059–1064.
<https://doi.org/10.1016/j.cherd.2009.02.001>
- Brown, L.D., Ulrich, A.C., 2015. Oil sands naphthenic acids: A review of properties, measurement, and treatment. *Chemosphere*.
<https://doi.org/10.1016/j.chemosphere.2015.02.003>
- Brunauer, S., Emmett, P., Teller, E., 1938. ADSORPTION OF GASES IN MULTIMOLECULAR LAYERS. *Journal of American Chemical Society* 60, 309–318. <https://doi.org/https://doi.org/10.1021/ja01269a023>
- Clemente, J.S., Fedorak, P.M., 2005. A review of the occurrence, analyses, toxicity, and biodegradation of naphthenic acids. *Chemosphere*.
<https://doi.org/10.1016/j.chemosphere.2005.02.065>
- Condon, James B, 2006. Surface Area and Porosity Determinations by Physisorption Measurement, Classical Theories and Quantum Theory, 1st ed. Elsevier, Amsterdam .
- Cossey, H.L., Batycky, A.E., Kaminsky, H., Ulrich, A.C., 2021. Geochemical stability of oil sands tailings in mine closure landforms. *Minerals* 11.
<https://doi.org/10.3390/min11080830>
- de Ridder, D.J., Villacorte, L., Verliefde, A.R.D., Verberk, J.Q.J.C., Heijman, S.G.J., Amy, G.L., van Dijk, J.C., 2010. Modeling equilibrium adsorption of organic micropollutants onto activated carbon. *Water Res* 44, 3077–3086.
<https://doi.org/10.1016/j.watres.2010.02.034>
- Eder, S., Müller, K., Azzari, P., Arcifa, A., Peydayesh, M., Nyström, L., 2021. Mass Transfer Mechanism and Equilibrium Modelling of Hydroxytyrosol Adsorption on Olive Pit–Derived Activated Carbon. *Chemical Engineering Journal* 404.
<https://doi.org/10.1016/j.cej.2020.126519>
- Energy Regulator, A., n.d. State of Fluid Tailings Management for Mineable Oil Sands, 2019.
- Foo, K.Y., Hameed, B.H., 2010. Insights into the modeling of adsorption isotherm systems. *Chemical Engineering Journal*.
<https://doi.org/10.1016/j.cej.2009.09.013>
- Ghosal, P.S., Gupta, A.K., 2017. Determination of thermodynamic parameters from Langmuir isotherm constant-revisited. *J Mol Liq* 225, 137–146.
<https://doi.org/10.1016/j.molliq.2016.11.058>
- Grewer, D.M., Young, R.F., Whittal, R.M., Fedorak, P.M., 2010. Naphthenic acids and other acid-extractables in water samples from Alberta: What is being

- measured? *Science of the Total Environment* 408, 5997–6010.
<https://doi.org/10.1016/j.scitotenv.2010.08.013>
- Han, X., Scott, A.C., Fedorak, P.M., Bataineh, M., Martin, J.W., 2008. Influence of molecular structure on the biodegradability of naphthenic acids. *Environ Sci Technol* 42, 1290–1295. <https://doi.org/10.1021/es702220c>
- Headley, J. V., Peru, K.M., Barrow, M.P., 2016. Advances in mass spectrometric characterization of naphthenic acids fraction compounds in oil sands environmental samples and crude oil - A review. *Mass Spectrom Rev.*
<https://doi.org/10.1002/mas.21472>
- Headley, J. V., Peru, K.M., Mohamed, M.H., Frank, R.A., Martin, J.W., Hazewinkel, R.R.O., Humphries, D., Gurprasad, N.P., Hewitt, L.M., Muir, D.C.G., Lindeman, D., Strub, R., Young, R.F., Grever, D.M., Whittall, R.M., Fedorak, P.M., Birkholz, D.A., Hindle, R., Reisdorph, R., Wang, X., Kasperski, K.L., Hamilton, C., Woudneh, M., Wang, G., Loescher, B., Farwell, A., Dixon, D.G., Ross, M., Dos Santos Pereira, A., King, E., Barrow, M.P., Fahlman, B., Bailey, J., McMartin, D.W., Borchers, C.H., Ryan, C.H., Toor, N.S., Gillis, H.M., Zuin, L., Bickerton, G., McMaster, M., Sverko, E., Shang, D., Wilson, L.D., Wrona, F.J., 2013. Chemical fingerprinting of naphthenic acids and oil sands process waters-A review of analytical methods for environmental samples. *J Environ Sci Health A Tox Hazard Subst Environ Eng.* <https://doi.org/10.1080/10934529.2013.776332>
- Ighalo, J.O., Iwuozor, K.O., Igwegbe, C.A., Adeniyi, A.G., 2021. Verification of pore size effect on aqueous-phase adsorption kinetics: A case study of methylene blue. *Colloids Surf A Physicochem Eng Asp* 626.
<https://doi.org/10.1016/j.colsurfa.2021.127119>
- Inglezakis, V.J., Zorpas, A.A., 2012. Heat of adsorption, adsorption energy and activation energy in adsorption and ion exchange systems. *Desalination Water Treat* 39, 149–157. <https://doi.org/10.1080/19443994.2012.669169>
- Iranmanesh, S., Harding, T., Abedi, J., Seyedeyn-Azad, F., Layzell, D.B., 2014. Adsorption of naphthenic acids on high surface area activated carbons. *J Environ Sci Health A Tox Hazard Subst Environ Eng* 49, 913–922.
<https://doi.org/10.1080/10934529.2014.894790>
- Islam, M.S., McPhedran, K.N., Messele, S.A., Liu, Y., Gamal El-Din, M., 2018. Isotherm and kinetic studies on adsorption of oil sands process-affected water organic compounds using granular activated carbon. *Chemosphere* 202, 716–725. <https://doi.org/10.1016/j.chemosphere.2018.03.149>
- Jagiello, J., Olivier, J.P., 2009. A simple two-dimensional NLDFT model of gas adsorption in finite carbon pores. application to pore structure analysis.

- Journal of Physical Chemistry C 113, 19382–19385.
<https://doi.org/10.1021/jp9082147>
- Kang, S., Jung, J., Choe, J.K., Ok, Y.S., Choi, Y., 2018. Effect of biochar particle size on hydrophobic organic compound sorption kinetics: Applicability of using representative size. *Science of the Total Environment* 619–620, 410–418. <https://doi.org/10.1016/j.scitotenv.2017.11.129>
- Kannel, P.R., Gan, T.Y., 2012. Naphthenic acids degradation and toxicity mitigation in tailings wastewater systems and aquatic environments: A review. *J Environ Sci Health A Tox Hazard Subst Environ Eng*.
<https://doi.org/10.1080/10934529.2012.629574>
- Li, C., Fu, L., Stafford, J., Belosevic, M., Gamal El-Din, M., 2017. The toxicity of oil sands process-affected water (OSPW): A critical review. *Science of the Total Environment*. <https://doi.org/10.1016/j.scitotenv.2017.06.024>
- Lima, É.C., Dehghani, M.H., Guleria, A., Sher, F., Karri, R.R., Dotto, G.L., Tran, H.N., 2021. Adsorption: Fundamental aspects and applications of adsorption for effluent treatment, in: *Green Technologies for the Defluoridation of Water*. Elsevier, pp. 41–88. <https://doi.org/10.1016/B978-0-323-85768-0.00004-X>
- Liu, Y., 2009. Is the free energy change of adsorption correctly calculated? *J Chem Eng Data* 54, 1981–1985. <https://doi.org/10.1021/je800661q>
- Marczewski, A.W., Seczkowska, M., Deryło-Marczewska, A., Blachnio, M., 2016. Adsorption equilibrium and kinetics of selected phenoxyacid pesticides on activated carbon: effect of temperature. *Adsorption* 22, 777–790.
<https://doi.org/10.1007/s10450-016-9774-0>
- Marsh, Harry., Rodríguez-Reinoso, F., 2006. *Activated carbon*. Elsevier.
- Martinez-Iglesias, A., Niasar, H.S., Xu, C.C., Ray, M.B., 2015. Adsorption of model naphthenic acids in water with granular activated carbon. *Adsorption Science and Technology* 33, 881–894. <https://doi.org/10.1260/0263-6174.33.10.881>
- Mônaco, F.S., de Aguiar, D.V.A., Oliveira, G. de A.R., Vaz, B.G., Lião, L.M., de Andrade, L.A., Ostroski, I.C., 2022. Adsorption of organic acids from offshore produced water using microporous activated carbon from babassu pericarp: a low-cost alternative. *Chem Eng Commun*.
<https://doi.org/10.1080/00986445.2022.2045281>
- Niasar, H.S., Das, S., Xu, C. (Charles), Ray, M.B., 2019. Continuous column adsorption of naphthenic acids from synthetic and real oil sands process-affected water (OSPW) using carbon-based adsorbents. *Chemosphere* 214, 511–518. <https://doi.org/10.1016/j.chemosphere.2018.09.078>

- Niasar, H.S., Li, H., Das, S., Kasanneni, T.V.R., Ray, M.B., Xu, C. (Charles), 2018. Preparation of activated petroleum coke for removal of naphthenic acids model compounds: Box-Behnken design optimization of KOH activation process. *J Environ Manage* 211, 63–72. <https://doi.org/10.1016/j.jenvman.2018.01.051>
- Niasar, H.S., Li, H., Kasanneni, T.V.R., Ray, M.B., Xu, C.C., 2016. Surface amination of activated carbon and petroleum coke for the removal of naphthenic acids and treatment of oil sands process-affected water (OSPW). *Chemical Engineering Journal* 293, 189–199. <https://doi.org/10.1016/j.cej.2016.02.062>
- Ntakirutimana, S., Tan, W., Wang, Y., 2019. Enhanced surface activity of activated carbon by surfactants synergism. *RSC Adv* 9, 26519–26531. <https://doi.org/10.1039/c9ra04521j>
- Nuhnen, A., Janiak, C., 2020. A practical guide to calculate the isosteric heat/enthalpy of adsorption: Via adsorption isotherms in metal-organic frameworks, MOFs. *Dalton Transactions*. <https://doi.org/10.1039/d0dt01784a>
- Piccin, J.S., Cadaval, T.R.S.A., De Pinto, L.A.A., Dotto, G.L., 2017. Adsorption isotherms in liquid phase: Experimental, modeling, and interpretations, in: *Adsorption Processes for Water Treatment and Purification*. Springer International Publishing, pp. 19–51. https://doi.org/10.1007/978-3-319-58136-1_2
- Plazinski, W., Dziuba, J., Rudzinski, W., 2013. Modeling of sorption kinetics: The pseudo-second order equation and the sorbate intraparticle diffusivity. *Adsorption* 19, 1055–1064. <https://doi.org/10.1007/s10450-013-9529-0>
- Quinlan, P.J., Tam, K.C., 2015. Water treatment technologies for the remediation of naphthenic acids in oil sands process-affected water. *Chemical Engineering Journal*. <https://doi.org/10.1016/j.cej.2015.05.062>
- Rowland, S.J., Scarlett, A.G., Jones, D., West, C.E., Frank, R.A., 2011a. Diamonds in the rough: Identification of individual naphthenic acids in oil sands process water. *Environ Sci Technol* 45, 3154–3159. <https://doi.org/10.1021/es103721b>
- Rowland, S.J., West, C.E., Scarlett, A.G., Jones, D., Frank, R.A., 2011b. Identification of individual tetra- and pentacyclic naphthenic acids in oil sands process water by comprehensive two-dimensional gas chromatography/mass spectrometry. *Rapid Communications in Mass Spectrometry* 25, 1198–1204. <https://doi.org/10.1002/rcm.4977>
- Saha, P., Chowdhury, S., 2011. 6 Insight Into Adsorption Thermodynamics, in: Tadashi, M. (Ed.), *Thermodynamics*. <https://doi.org/10.5772/13474>

- Salvestrini, S., Leone, V., Iovino, P., Canzano, S., Capasso, S., 2014. Considerations about the correct evaluation of sorption thermodynamic parameters from equilibrium isotherms. *Journal of Chemical Thermodynamics* 68, 310–316. <https://doi.org/10.1016/j.jct.2013.09.013>
- Sarkar, B., 2013. Adsorption of Single-ring Model Naphthenic Acid from Oil Sands Tailings Pond Water Using Petroleum Coke-Derived Activated Carbon.
- Skelly, E., Robinson, J., Frame II, G., 2014. Undergraduate Instrumental Analysis, 7th ed. CRC Press. <https://doi.org/https://doi.org/10.1201/b15921>
- Small, C.C., Ulrich, A.C., Hashisho, Z., 2012. Adsorption of Acid Extractable Oil Sands Tailings Organics onto Raw and Activated Oil Sands Coke. *Journal of Environmental Engineering* 138, 833–840. [https://doi.org/10.1061/\(asce\)ee.1943-7870.0000543](https://doi.org/10.1061/(asce)ee.1943-7870.0000543)
- Smith, B.E., Lewis, C.A., Belt, S.T., Whitby, C., Rowland, S.J., 2008. Effects of alkyl chain branching on the biotransformation of naphthenic acids. *Environ Sci Technol* 42, 9323–9328. <https://doi.org/10.1021/es801922p>
- Sophia A., C., Lima, E.C., 2018. Removal of emerging contaminants from the environment by adsorption. *Ecotoxicol Environ Saf* 150, 1–17. <https://doi.org/10.1016/j.ecoenv.2017.12.026>
- Stevie, F.A., Donley, C.L., 2020. Introduction to x-ray photoelectron spectroscopy. *Journal of Vacuum Science & Technology A: Vacuum, Surfaces, and Films* 38. <https://doi.org/10.1116/6.0000412>
- Strong, O.K.L., France, H.E., Scotland, K., Wright, K., Vreugdenhil, A.J., 2023a. Selenite Adsorption and Reduction via Iron(II) Impregnated Activated Carbon Produced from the Phosphoric Acid Activation of Construction Waste Wood. *Arch Environ Contam Toxicol* 85, 485–497. <https://doi.org/10.1007/s00244-023-01032-y>
- Strong, O.K.L., Nazari, E., Roy, T., Scotland, K., Pede, P.R., Vreugdenhil, A.J., 2023b. Transforming micropores to mesopores by heat cycling KOH activated petcoke for improved kinetics of adsorption of naphthenic acids. *Heliyon* 9. <https://doi.org/10.1016/j.heliyon.2023.e13500>
- Suncor Energy, n.d. Syncrude Pit Lake Monitoring and Research Report.
- Suresh Kumar, P., Korving, L., Keesman, K.J., van Loosdrecht, M.C.M., Witkamp, G.J., 2019. Effect of pore size distribution and particle size of porous metal oxides on phosphate adsorption capacity and kinetics. *Chemical Engineering Journal* 358, 160–169. <https://doi.org/10.1016/j.cej.2018.09.202>

- Tan, K.L., Hameed, B.H., 2017. Insight into the adsorption kinetics models for the removal of contaminants from aqueous solutions. *J Taiwan Inst Chem Eng* 74, 25–48. <https://doi.org/10.1016/j.jtice.2017.01.024>
- Total Organic Carbon Analyzer TOC-VCPH/CPN User's Manual, 2010. . Japan.
- Tran, H.N., Thanh Trung, N.P., Lima, E.C., Bollinger, J.C., Dat, N.D., Chao, H.P., Juang, R.S., 2023. Revisiting the calculation of thermodynamic parameters of adsorption processes from the modified equilibrium constant of the Redlich–Peterson model. *Journal of Chemical Technology and Biotechnology* 98, 462–472. <https://doi.org/10.1002/jctb.7258>
- Tran, H.N., You, S.J., Chao, H.P., 2016. Thermodynamic parameters of cadmium adsorption onto orange peel calculated from various methods: A comparison study. *J Environ Chem Eng* 4, 2671–2682. <https://doi.org/10.1016/j.jece.2016.05.009>
- Tran, H.N., You, S.J., Hosseini-Bandegharai, A., Chao, H.P., 2017. Mistakes and inconsistencies regarding adsorption of contaminants from aqueous solutions: A critical review. *Water Res.* <https://doi.org/10.1016/j.watres.2017.04.014>
- Vanore, P., Coppola, E., Iovino, P., Leone, V., Salvestrini, S., Capasso, S., 2017. Sorption thermodynamics of organic pollutants onto zeolitic tuff: Isosteric and standard enthalpy. *Journal of Water Chemistry and Technology* 39, 228–232. <https://doi.org/10.3103/S1063455X17040087>
- Veksha, A., Bhuiyan, T.I., Hill, J.M., 2016. Activation of aspen wood with carbon dioxide and phosphoric acid for removal of total organic carbon from oil sands produced water: Increasing the yield with bio-oil recycling. *Materials* 9. <https://doi.org/10.3390/ma9010020>
- Wang, J., Guo, X., 2020. Adsorption kinetic models: Physical meanings, applications, and solving methods. *J Hazard Mater.* <https://doi.org/10.1016/j.jhazmat.2020.122156>
- Wang, N., Chelme-Ayala, P., Perez-Estrada, L., Garcia-Garcia, E., Pun, J., Martin, J.W., Belosevic, M., Gamal El-Din, M., 2013. Impact of ozonation on naphthenic acids speciation and toxicity of oil sands process-affected water to vibrio fischeri and mammalian immune system. *Environ Sci Technol* 47, 6518–6526. <https://doi.org/10.1021/es4008195>
- Worch, E., 2012. Adsorption Technology in Water Treatment Fundamentals, Processes, and Modeling. De Gruyter. <https://doi.org/https://doi.org/10.1515/9783110240238.41>

- Wu, C., De Visscher, A., Gates, I.D., 2019. On naphthenic acids removal from crude oil and oil sands process-affected water. *Fuel*. <https://doi.org/10.1016/j.fuel.2019.05.091>
- Wu, J., Montes, V., Virla, L.D., Hill, J.M., 2018. Impacts of amount of chemical agent and addition of steam for activation of petroleum coke with KOH or NaOH. *Fuel Processing Technology* 181, 53–60. <https://doi.org/10.1016/j.fuproc.2018.09.018>
- Xu, X., Pliego, G., Zazo, J.A., Sun, S., García-Muñoz, P., He, L., Casas, J.A., Rodriguez, J.J., 2017. An overview on the application of advanced oxidation processes for the removal of naphthenic acids from water. *Crit Rev Environ Sci Technol* 47, 1337–1370. <https://doi.org/10.1080/10643389.2017.1348113>
- Yorgun, S., Yildiz, D., 2015. Preparation and characterization of activated carbons from Paulownia wood by chemical activation with H₃PO₄. *J Taiwan Inst Chem Eng* 53, 122–131. <https://doi.org/10.1016/j.jtice.2015.02.032>

Appendix

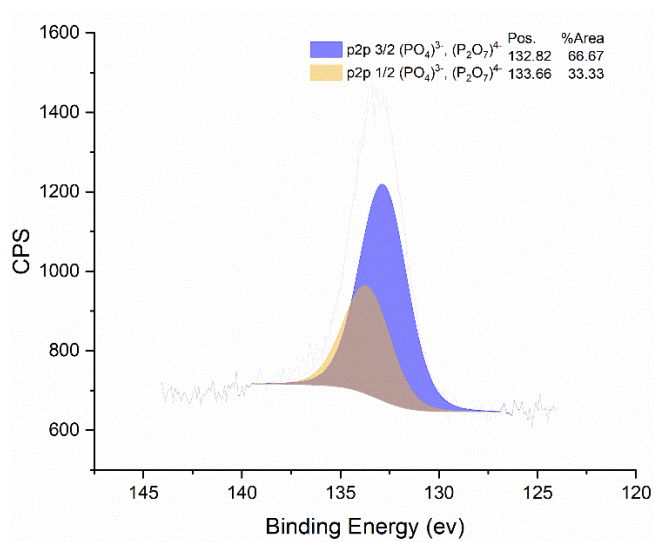


Figure A.1: p 2p high resolution scan of HAC.